Star formation history and evolution of gas-rich dwarf galaxies in the Centaurus A group⋆

M. Grossi[1,2], M. J. Disney[1], B. J .Pritzl[3], P. M. Knezek[4,5]†, J. S. Gallagher[6], R. F. Minchin[7] and K. C. Freeman[8]

[1] *School of Physics and Astronomy, Cardiff University, Cardiff, CF24 3YB, UK*
[2] *Istituto di Fisica dello Spazio Interplanetario INAF-IFSI, Via del Fosso del Cavaliere 100, 00133 Roma, Italy*
[3] *Macalester College, 1600 Grand Avenue, Saint Paul, MN 55105, USA*
[4] *National Optical Astronomy Observatory, P.O. Box 26732, Tucson, AZ 85726, USA*
[5] *WIYN Consortium, Inc., P.O. Box 26732, Tucson, AZ 85726, USA*
[6] *Dep. of Astronomy, University of Wisconsin, Madison, WI 53706-1582, USA*
[7] *Arecibo Observatory, HC03 Box 53995, PR 00612, USA*
[8] *Research School of Astronomy and Astrophysics, Mount Stromlo Oservatory, Cotter Road, Weston, ACT 2611, Australia*

6 November 2006

ABSTRACT

We analyse the properties of three unusual dwarf galaxies in the Centaurus A group discovered with the HIPASS survey. From their optical morphology they appear to be low surface brightness dwarf spheroidals, yet they are gas-rich ($M_{HI}/L_B >$ 1) with gas-mass-to-stellar light ratios larger than typical dwarf irregular galaxies. Therefore these systems appear different from any dwarfs of the Local Group. They should be favoured hosts for starburst, whereas we find a faint star formation region in only one object. We have obtained 21-cm data and Hubble Space Telescope photometry in V and I bands, and have constructed Colour Magnitude Diagrams (CMDs) to investigate their stellar populations and to set a constraint on their age. From the comparison of the observed and model CMDs we infer that all three galaxies are at least older than 2 Gyr (possibly even as old as 10 Gyr) and remain gas-rich because their star formation rates (SFRs) have been very low ($\lesssim 10^{-3}\ M_\odot\ \mathrm{yr}^{-1}$) throughout. In such systems, star formation (SF) appears to have been sporadic and local, though one object (HIPASS J1321–31) has a peculiar red plume in its CMD suggesting that many of its stars were formed in a "miniburst" 300 - 500 Myr ago. The question of why there are no similar dwarf galaxies in the Local Group remains open.

Key words: galaxies: dwarfs — galaxies: evolution — galaxies: stellar content)

1 INTRODUCTION

1.1 Overview

Galaxy evolution is related to the rate at which the gas content is transformed into stars. Along the Hubble sequence this process appears to be very efficient, and a clear trend holds between gas content and morphological type with gas-poor early-type galaxies at one end of the sequence and gas-rich late-type Sd spirals at the other (Roberts & Haynes 1994). The gas-mass-to-luminosity ratio (M_{HI}/L_B) is generally taken as a measure of how gas-rich a galaxy is, with most optically-selected galaxies having $M_{HI}/L_B < 1$ in solar units. However, *blind* neutral hydrogen surveys such as HIPASS (Meyer et al. 2004), HIJASS (Lang et al. 2003) and HIDEEP (Minchin et al. 2003) have found large numbers of gas-rich objects where the gas component is dominant

⋆ Based on observations with: the NASA/ESA *Hubble Space Telescope*, obtained at the Space Telescope Science Institute, which is operated by the Associations of Universities for Research in Astronomy (AURA), Inc., under NASA contract NAS 5-26555; the Australia Telescope Compact Array which is part of the Australia Telescope, funded by the Commonwealth of Australia for operation as a National Facility managed by CSIRO.
† Visiting Astronomer, Kitt Peak National Observatory, National Optical Astronomy Observatories, which is operated by the Association of Universities for Research in Astronomy, Inc. (AURA) under cooperative agreement with the National Science Foundation.

compared to the stellar one ($M_{HI}/L_B > 1$). Such objects make up about 30% of the detections in these surveys (e.g. Koribalski et al. 2004; Minchin et al. 2004).

In the optical, gas-rich galaxies often have low surface brightnesses (LSBs) and low luminosities, but they can also be found with high star formation rates. Blue compact dwarfs are gas-rich objects undergoing an intense burst of star formation, even though their HI mass-to-light ratios are hardly very high, being usually in the range $0.1 \leqslant M_{HI}/L_B \leqslant 2.0$ in solar units. It is not only dwarf galaxies that can be gas-rich, HI massive systems with high M_{HI}/L_B ratios have been found in HIPASS (Kilborn et al. 2002). Nevertheless the highest values of M_{HI}/L_B are found in objects that appear in the optical as LSB, low luminosity dwarf galaxies (van Zee et al. 1997a,b, van Zee 2001a; Warren et al. 2004) and such systems are the subject of this paper.

We present the properties of three gas-rich dwarf galaxies ($M_{HI} \lesssim 10^7\ M_\odot$) recently discovered at 21-cm in the Centaurus A group (Banks et al. 1999, Minchin et al. 2003). To all optical appearances they look like dwarf spheroidals but their gas-to-stellar ratios (M_{HI}/L_B) range from 1.4 to 5 in solar units which means they have no similar counterparts in the Local Group (LG). They are puzzling because, in principle, they represent an ideal environment for SF, given their large gas fractions and their location in a fairly populated group such as Centaurus A. Yet their M_{HI}/L_B ratios indicate that a large fraction of the galactic gas reservoir has not been converted into stars yet.

Are we finding a new class of galaxies? Are they young? Are there any common properties with the well studied dwarf systems of the LG? Do these gas-rich dwarfs show star formation histories (SFHs) similar among themselves, or are they different one from the other? The aim of this analysis is to try to understand some of these issues.

One possible explanation is that they represent a local population of *young* (< 1 Gyr) galaxies, which are gas-rich because they have not existed long enough to transform their gas into stars. The presence of nearby young systems has been under debate for years until the recent discovery that the best candidate for a nearby young galaxy, the blue compact dwarf (BCD) galaxy I Zw 18 (12.6 Mpc $< d <$ 15 Mpc), does not contain a population of stars older than $\sim$ 500 Myr (Izotov & Thuan 2004). Being at a distance of less than 5 Mpc, the Centaurus A dwarfs may represent ideal candidate young galaxies to study.

Alternatively, these systems could be *old* galaxies, that formed their first stellar populations several Gyr ago, but have evolved at a slower rate compared to "normal" Local Group galaxies i.e. they are in some sense *"retarded"*. If this is the case, then what prevents stars from forming in such objects? If one could answer this question we might learn something about galaxy evolution in general.

In order to investigate the Star Formation Histories (SFHs) of these dwarf galaxies we have obtained Hubble Space Telescope (HST) images in V and I from which we have built CMDs. These are compared to 21-cm maps obtained with the Australia Telescope Compact Array (ATCA).

This paper will proceed as follows: first an overview of the Centaurus A group is given in the remaining part of this introductory section (§1.2). In section 2 we describe both the 21-cm and the optical data we have obtained. In sections 3, 4, 5 we analyse the three dwarfs, HIPASS J1337–39, HIDEEP J1337–3320 and HIPASS J1321–31 individually. Finally our results will be summarised in §6. In §7 we present our conclusions.

1.2 The Centaurus A group

The Centaurus A group is a heterogeneous assembly of early to late-type galaxies at a distance of between 3.5 and 4.5 Mpc, covering about 1000 square degrees of sky. The two largest galaxies in the group are NGC 5128 (Cen A), the nearest early-type giant and a very active radio galaxy, and the spiral NGC 5236 (M 83)

The distance of the group was originally set by de Vaucouleurs at $d = 4.0$ Mpc (1975). Soria et al. (1996) placed NGC 5128 at 3.6 ± 0.2 Mpc using the tip of the red giant branch (TRGB) while, also from the TRGB, Harris et al. (1998) found a distance of 3.9 ± 0.2 Mpc.

NGC 5236 appears to be more distant than NGC 5128: Thim et al. (2003) derived $d_{M83} = 4.5 \pm 0.3$ Mpc from Cepheid observations. Its close neighbour, NGC 5253 (angular separation 110 arcmin), is at $d = 4.0 \pm 0.3$ Mpc from Cepheid and SN Ia (Saha et al. 1995) measurements.

In recent years, the number of smaller galaxies associated with the group has increased greatly. Côté et al. (1997) added 20 dwarf galaxies (mainly gas-rich dwarf irregulars) of which 2 were newly identified. Four gas-rich neighbours were found around M 83 in this survey, but none near NGC 5128, presumably because its hot gaseous halo make Cen A a very hard environment for the "survival" of gas-rich satellites.

An HI survey of the group by Banks et al. (1999) added another ten members, five of which were previously known galaxies with wrong or no redshift measurements, and a deeper, smaller-area HI survey, HIDEEP (Minchin et al. 2003), added another new dwarf. All of the new six detections appeared to have optical counterparts, although very faint ($M \sim -11$) and LSB ($\mu_0^B \gtrsim 24$ mag arcsec^{-2}).

Another optical survey covering the same area as Côté and collaborators, aimed at finding exclusively dwarf elliptical candidates, added 13 new dSph members to the group (Jerjen et al. 2000a, 2000b). The survey led also to the addition of one more dIrr galaxies (AM1318-444).

Seven more members have been included in the group by Karachentsev et al. (2002) with a survey of nearby dwarf galaxy candidates which is part of the Hubble Space Telescope snapshot (SNAP) program. The majority of the targets were taken from the results of an all-sky search for nearby dwarf galaxies, based on the POSS II and ESO/SERC plates and were mainly dwarf spheroidal, LSB galaxies.

To date, 62 candidate members of the group have been classified, and a measure of the distance is available for about thirty objects (Karachentsev 2005).

As regards the inner structure of the Centaurus A group, de Vaucouleurs (1975), Tully (1987), Van den Bergh (2000a), consider that all the brightest members form a single group, while Karachentsev (1996) argues that the two massive galaxies, NGC 5128 (CenA) and NGC 5236 (M 83) are the centres of two separate subgroups (Karachentsev et al. 2002), at a distance $d_{CenA} = 3.66 \pm 0.07$ Mpc and $d_{M83} = 4.57 \pm 0.05$ Mpc respectively. Moreover the M 83

group is moving away from Cen A at a relative radial velocity of 55 $\mathrm{km\,s^{-1}}$(Karachentsev et al. 2002).

Whether the two groups are separated or not partly depends on the assumed distance of NGC 5128, which is found to range in the literature between 3.6 and 4.0 Mpc. However, Karachentsev and collaborators find a clear distinction between objects with average distance around 3.6 Mpc and those whose average distance is 4.5 Mpc: a result that strengthens the two subgroups interpretation.

To conclude, the Centaurus A complex of galaxies appears as a very rich environment within the Local Volume, with a variety of members spanning different morphological types, hardly found in other nearby groups. Sculptor, for instance, lacks both early-type members and bright Milky-Way-like spiral galaxies, while the M 81 group has about 28 members (with only one large spiral and 23 dwarf candidate members) but in contrast with Centaurus A, it is a very compact group.

2 OBSERVATIONS AND DATA REDUCTION

Four among the six new gas-rich dwarf galaxies from HIPASS and HIDEEP were chosen to be followed up with the HST's Wide Field Planetary Camera 2 (WFPC2) and at 21-cm with ATCA. The remaining two (HIPASS J1348-37, HIPASS J1351-47) have both high M_{HI}/L_B ratios, respectively 2.7 and 3.9, but they were not included in the list because they had been already observed with the WFPC2 as part of the SNAP survey.

2.1 ATCA HI observations

Observations were carried out with ATCA in a 750-m configuration in May 2001 and in a 1.5-km configuration in October 2001. Both sets of observations had an integration time of 12 hours per source and used a bandwidth of 4 MHz, divided into 1024 channels to give a velocity resolution of 0.8 $\mathrm{km\,s^{-1}}$. PKS 1934-638 was used as the flux calibrator and PKS 1320-1446 as the phase calibrator.

The first run gave short-baseline data that were then combined with the long-baseline ones to give a good compromise between sensitivity and resolution. The first data set also allowed us to check the reality of the sources; one of the objects (HIPASS J1328-30) turned out to be a more distant uncatalogued LSB galaxy at $v_{opt} \sim 8100$ $\mathrm{km\,s^{-1}}$which overlaps a local high velocity cloud with $v_{helio} \sim 200$ $\mathrm{km\,s^{-1}}$. This was confirmed by the WFPC2 image of this object (Fig. 1). The galaxy shows a compact fairly bright core, with an extended LSB disc with spiral arms. The corresponding dereddened total magnitude is $m_{I,tot} = 11.65 \pm 0.03$ mag. This galaxy was therefore not observed in the second run.

Data reduction was carried out in MIRIAD. For HIPASS J1321–31 and HIDEEP J1337–3320 a robust setting of 0.5 was used, giving a lower noise level at the expense of some angular resolution. This gave a noise of 3 mJy per channel with beam-sizes $\sim 57'' \times 29''$(HIPASS J1321–31) and $\sim 59'' \times 32''$(HIDEEP J1337–3320). For HIPASS J1337–39, uniform weighting was used to obtain the best angular resolution. This gave a noise of 5 mJy per channel and a beam-size $\sim 31'' \times 24''$.

ATCA and single dish fluxes obtained by the HIPASS survey with the Parkes telescope have been compared to check if a component of the flux was missing in the interferometric detections, but we found that variations are in the order of the 10%, consistent with the errors in HIPASS fluxes.

The main optical and HI properties of the three HIPASS dwarfs are shown in Table 1.

2.2 WFPC2 optical observations

The three targets were followed up with WFPC2 in June 2001 through the filters F555W and F814W. These two filters were chosen for ease of transformation to the Johnson/Cousin V and I system which is the standard for observing both old and young stellar populations. To get the largest spatial coverage possible the galaxies were centred in the WF3 chip of the camera, with a spatial sampling of $0''.1$ per pixel and a field of view of $80'' \times 80''$. Four orbits were assigned to each target for a total of 5000 s (F555W) and 5200 s (F814W).

The frames were debiased, zero-corrected, dark-subtracted and flat-fielded by the Space Telescope Science Institute (STScI) pipeline process before being made available. They were then combined with the task CRREJ in IRAF[1] to remove contamination by cosmic rays on the frames. The photometry was done using the IRAF version of the package DAOPHOT and ALLFRAME (Stetson 1987). A parallel analysis of the data (Pritzl et al. 2003) has been performed by our collaborators at the National Optical Astronomy Observatory (NOAO) using the stand-alone version of DAOPHOT. A preliminary selection of stars with $S/N > 3$ was performed with the automatic star-finding algorithm DAOFIND and their magnitudes obtained with the task PHOT using an aperture radius of 2.0 pixels. An empirical point-spread function was built with the task PSF by selecting several isolated and bright stars in each frame containing the galaxies. The instrumental magnitudes were measured with the ALLSTAR algorithm (Stetson 1994) by fitting the point-spread function to the brightness profile of any given object.

When measuring the photometry of stars in a crowded field some mistakes and wrong detections are inevitable. Defective pixels, cosmic rays, background objects, and stellar blends can "pollute" the output of the measured photometry performed by ALLSTAR. However the routine produces indices that give an indication of the reliability of the fit and provide a tool to flag and reject dubious detections.

These indices are: χ, the square root of the standard χ^2 goodness-of-fit index and represents a dimensionless measure of the agreement between the measured brightness profile and the model PSF for any given stellar detection. The residuals of the fitting, σ, that are representative of the errors on the derived instrumental magnitudes. Lastly, *sharp* is a first order estimate of the intrinsic angular radius of a resolved source: if the PSF has a characteristic radius s_{PSF} and the measured image profile has a radius s_{obs}, $sharp^2 = |s_{obs}^2 - s_{PSF}^2|^2$. *Sharp* values should be tightly

[1] IRAF is distributed by the National Optical Astronomy Observatories, which are operated by the Association of Universities for Research in Astronomy, Inc., under contract to the National Science Foundation.

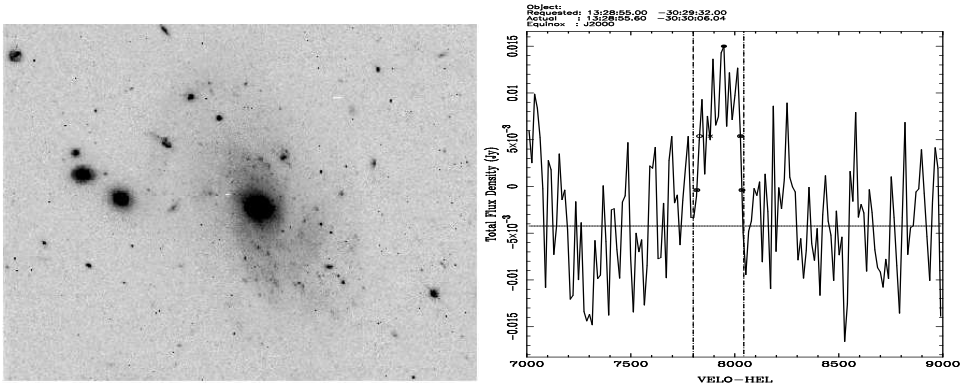

Figure 1. HIPASS J1328-31. *Left:* WFPC2 image taken with the filter F814W. *Right:* 21-cm spectrum taken from the HIDEEP survey (Minchin et al. 2003).

Table 1. Observed properties of the three Centaurus A dwarfs

SOURCE	RA J2000	DEC J2000	v_{helio} (km s^{-1})	r (kpc)	m_B	M_B	M_{HI} $10^7 M_\odot$	M_{HI}/L_B $(M_\odot/L_\odot)$
HIPASS J1337–39	13:37:26	-39:52:15	491	0.40	16.1	-12.6	3.9	2.1
HIDEEP J1337–3320	13:37:01	-33:21:47	590	0.22	17.5	-10.9	0.5	1.4
HIPASS J1321–31	13:21:06	-31:32:25	572	0.76	17.1	-11.7	3.7	4.9

clustered around zero for bright stars, while the deviation from zero increases for fainter stars.

Therefore, to minimise the number of false detections we have included only stars with $-0.5 < sharp < 0.5$. For stars with poor photometry (errors > 0.1 mag), an additional criterion of $\chi < 2$ was applied. This choice should provide a representative sample of detections for each dwarf, excluding both objects smaller than the size of a star, such as cosmic rays or image defects, and extended objects like galaxies, HII regions, stellar blends and any remaining blemishes. We have shown in Fig. 2 the plots of V and I magnitudes versus their relative photometric errors calculated by ALLSTAR, after having applied the rejection criteria.

The transformation from the F555W and F814W magnitudes to the Johnson-Cousin system was performed using the iterative procedure described in Holtzmann et al.(1995a) and the colour terms given in their Table 7. We determined the aperture corrections from the PSF fitting photometry to the 5 pixels aperture considered in Holtzmann et al. (1995a). Further corrections were applied for the exposure time, the gain factors and the charge transfer efficiency (CTE), using the equations derived by Dolphin (2000a). The final lists of stars were matched in both filters assuming a matching radius of 1 pixel ($0.1''$).

The completeness or our photometry has been tested by adding artificial stars of known I and V magnitudes to the original frames using the ADDSTAR algorithm of DAOPHOT. For each 0.5 bin of magnitude we have added 400 stars. To avoid overcrowding effects we have created four images per each bin and included 100 uniformly distributed artificial stars in each of them. Each frame was then processed in exactly the same way as the original images. The resulting photometry has been matched with the original list of stars and magnitudes created with ADDSTAR. The percentage of recovered stars (shown in Fig. 3) indicate that completeness is around 50% for $V = 27.2$ mag and $I = 26.2$ mag for HIPASS J1337–39, and is approximately the same for the other galaxies.

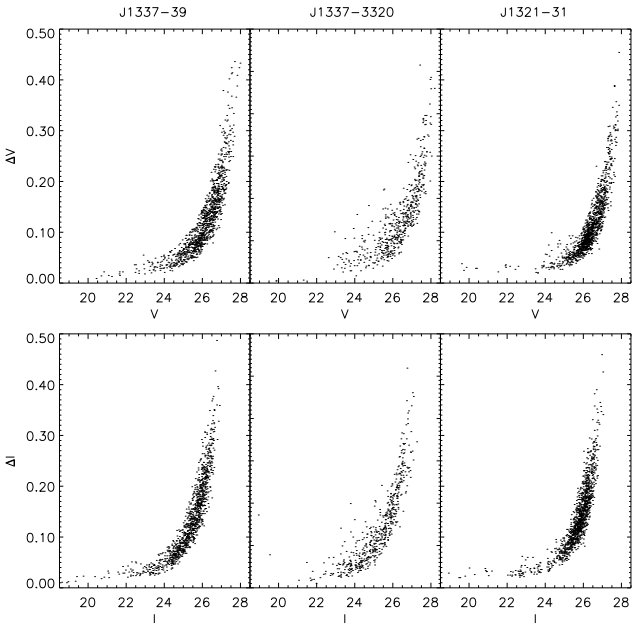

Figure 2. HIPASS J1337–39: Plot of photometric errors vs. apparent visual magnitudes in both V (*upper panel*) and I (*lower panel*) bands after applying the rejection criteria and transforming to the Johnson system.

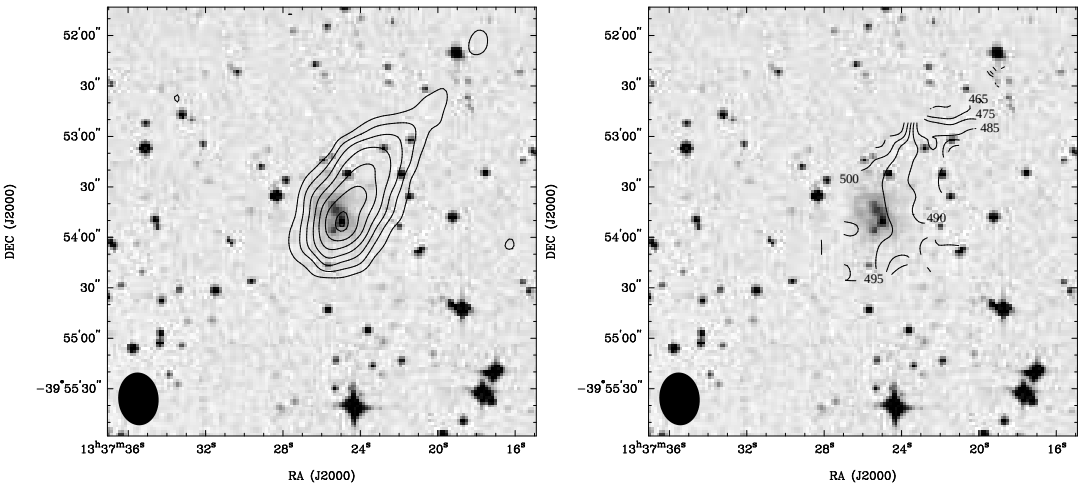

Figure 4. *Left:* HI density contour maps of HIPASS J1337–39 overlaid on the Digital Sky survey field including the galaxy. The contour levels are: 2.5, 5.0, 7.5, 10, 12.5, 15, 17.5 $\times 10^{20}$ cm^{-2}. *Right:* The HI velocity field: contours are in the range between 465 km s^{-1} and 500 km s^{-1}. The beam size is shown at the bottom left corner of the image.

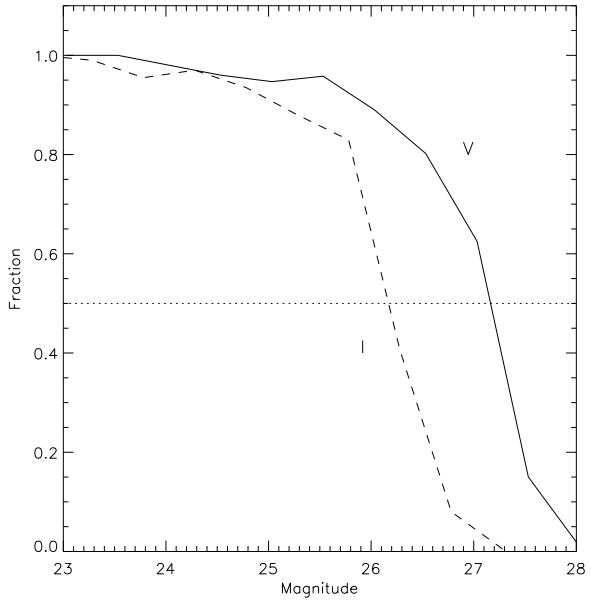

Figure 3. Photometry completeness expressed in percentage of recovered stars. Since we do not find large variations between the three fields, for the sake of clarity here we show only the case of HIPASS J1337–39. The horizontal dotted line represents the 50% level.

2.3 Hα observations

Direct Hα imaging observations were made at the WIYN Observatory[2] 3.5 m telescope. The data were taken on 29 and 30 May 2002 with MiniMo, which has two SITe 4096 x 2048 thinned CCDs. The pixel scale is 0.14 arcsec/pixel and the field of view is 9.6 arcminutes. Broadband R images were made using a Harris filter, and narrowband Hα imaging was done using a filter centered at 6570 $\AA$ and 73 $\AA$ wide. For each dwarf galaxy the integrations time were 3 minutes in R, and 30 minutes (3 images of 10 minutes each) in Hα. The Landolt standard field PG1323-086 (Landolt 1992) was observed each night in both filters, along with the spectrophotometric standard Cyg OB2 No. 9 (Massey et al. 1988).

Data processing was done using the MSCRED reduction tasks in IRAF. In order to estimate the Hα flux for each galaxy, the observations of the spectrophotometric standard Cyg OB2 No. 9 were used. Only the galaxy HIPASS J1337-39 was detected in emission. For HIDEEP J1337-33 and HIPASS J1321-31, the flux limit is derived by measuring the flux in the faintest detected stars in each image. For these galaxies, we estimate that the Hα flux is less than 7×10^{-16} ergs cm^{-2} sec^{-1}.

Then we have observed HIPASS J1337-39 with the Double Beam Spectrograph (DBS) on the 2.3 m telescope at the Siding Spring Observatory[3] to study the chemical abundance of the HII region and to obtain an independent measure of the metallicity. The DBS provides a spectral coverage of 3600 - 7000 Å.

Two exposures of 1337-39, each 2000 s long, were taken with both the blue and red grism. We performed the wavelength calibration using Neon - Argon lamps with exposures taken before and after the object observations. After the flux calibration (performed with the spectrophotometric standard EG21 and LTT3864; Hamuy et al. 1992, 1994), one-dimensional spectra were extracted from the two-dimensional images by summing up all the pixels enclosed in the profiles of the Hα line. The background and sky lines were subtracted by averaging a region on either side of the extraction window. We have then identified the main emission lines and measured their fluxes. The data were reduced with the IRAF package. The observed line intensities were corrected for interstellar extinction by comparing the ob-

[2] The WIYN Observatory is a joint facility of the University of Wisconsin-Madison, Indiana University, Yale University, and the National Optical Astronomy Observatories.

[3] The 2.3 meter Telescope is run by the Australian National University as part of the Research School of Astronomy and Astrophysics.

served and the expected hydrogen line ratios. Assuming the theoretical Balmer line value for case B recombination (Osterbrock 1989), we have determined the reddening constant $C(H\beta) = (\log R_0/R)/\phi(\lambda)$ where $R_0 = I_{\lambda,0}/I_{H\beta,0}$ is the theoretical H line ratios relative to Hβ, R is the observed ratio, $\phi(\lambda) = f(\lambda) - f(H\beta)$ is the extinction function relative to the Hβ line, where $f(\lambda) =< A(\lambda)/A(V) >$. For $A(\lambda)$ we have assumed the reddening law of Cardelli et al. (1989), with $R_V = 3.1$.

3 HIPASS J1337–39

Among the three dwarfs, J1337–39 is the only galaxy with ongoing star formation activity. With an HI mass of 3.9×10^7 $M_\odot$ and a total apparent magnitude $m_B = 16.1$ (Doyle et al. 2005), it has a gas-mass-to-stellar ratio $M_{HI}/L_B \simeq 2$ in solar units.

3.1 The neutral gas content

The neutral gas in J1337–39 (Fig. 4) shows a smooth distribution with a one-sided extension to the north west direction out to a projected radius of $1'30''$, or ~ 2 kpc at the assumed distance of 4.8 Mpc (see §3.5). J1337–39 has the highest average HI column density of the three dwarfs, and gas can be traced out to an HI column density of 2.5×10^{20} cm^{-2} . The overall high column density may explain why this is the only galaxy with ongoing star formation. The density peak is at $\sim 2 \times 10^{21}$ cm^{-2} in correspondence with the star forming regions and slightly offset from the optical centre of the galaxy (see Fig. 4).

The velocity field is shown in the right panel of Fig. 4. There is evidence of a small velocity gradient throughout the galaxy; the disc appears to be slowly rotating although the rotation is not very sharply defined. The velocity contours become rather irregular in the outer edge of the galaxy, in correspondence with the edge of the HI "tail", while around the main optical body the velocity field looks fairly regular.

From the 21-cm integrated flux we derive an HI mass $M_{HI} = 3.9 \times 10^7$ $M_\odot$, at a distance of 4.8 Mpc. The HI profile has a characteristic width $\Delta v_{20\%} \sim 50$ km s^{-1}. A rough estimate of the dynamical mass (without any inclination-angle correction) gives $M_{dyn} = V_R^2 \times R_{HI}/G \sim 4 \times 10^8$ $M_\odot$, and the ratio $M_{HI}/M_{dyn} \sim 0.1$ is similar to the sample of gas-rich dwarfs studied by van Zee et al. (1997a) and to what is found for ESO0215-G?009 ($M_{HI}/M_{dyn} = 0.11$), one of the most gas-rich galaxies ever detected with $M_{HI}/L_B = 22$ (Warren et al. 2004). Roberts & Haynes (1994) determined for their sample of Sm/Im galaxies a median value of 0.15.

The role of chaotic motions is in general more important in low mass galaxies (Young & Lo, 1996, Lo & Sargent 1993). As an estimate of the dispersion of the gas, in order to calculate the balance between rotation and chaotic motions, we have calculated the second moment with MIRIAD, defined as

$$\sigma = M_2 = \sqrt{\frac{\int I(v)(v - M_1)^2 dv}{\int I(v) dv}}$$

which corresponds to the intensity weighted velocity dispersion squared, where M_1 is the intensity weighted velocity defined as $\int I(v) v dv / \int I(v) dv$.

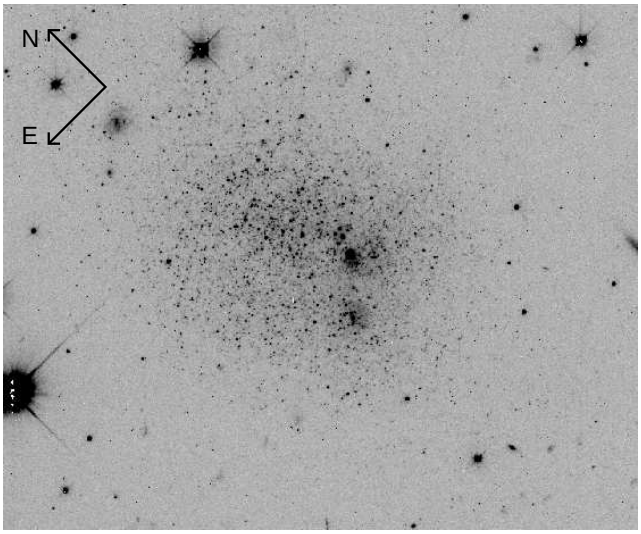

Figure 5. HIPASS J1337–39: The WFPC2 image of the galaxy taken with the filter F555W. The size of the frame is roughly $80''$. North is on the upper-left corner, and East on the lower-left one. Two nearby HII regions are clearly visible in the southern area of the galaxy.

For HIPASS J1337–39 the resulting velocity dispersion is $\sigma_v \simeq 10$ km s^{-1}. The velocity resolution of our data is ~ 1 km s^{-1}, so we are not measuring an instrumental effect. Although the velocity dispersion is comparable to the rotational velocity $V_R = 25$ km s^{-1}(without inclination-angle corrections), chaotic motions appear not to be dominant for this dwarf.

Finally we have inspected the immediate environment of the galaxy to search for possible companions within the ATCA primary beam ($\sim 30'$), but we have not detected any emission from other sources.

3.2 Optical properties and the oxygen abundance

The bulk of the stellar distribution (Fig. 5) shows an overall spherical symmetry, similar to that found in dSph galaxies. Outside the main spherical distribution, stars probably belonging to the dwarf extend north-south along the diagonal of the chip to the edges of the frame.

Star formation activity in this galaxy has been confirmed by Hα observations taken with the WIYN telescope and two nearby HII regions can be identified also from the WFPC2 image (Fig. 5), slightly offset from the optical centre.

The symmetric stellar distribution of J1337–39 resembles that of dwarf spheroidals, while the ongoing SF activity and the large gas fraction is more typical of dIrr galaxies.

Once Hα emission had been detected, observations with the Double Beam Spectrograph (DBS) on the 2.3 m telescope at the Siding Spring Observatory were taken to obtain an independent measure of the current metal abundance of the ISM. This allows us to break the age-metallicity degeneracy that represents the main difficulty in the study of the stellar populations from CMDs.

We detected a number of lines, including Hα, Hβ, OII

Table 2. Line flux ratios relative to Hβ. We also show the value of the reddening constant, $C(H\beta)$ and the Hα, Hβ fluxes.

Ionic species	$F(\lambda)/F(H\beta)$
[OII]	0.20 ± 0.06
Hβ	1. ± 0.05
[OIII](5007+4959)	3.10 ± 0.28
Hα	2.87 ± 0.20
$C(H\beta)$	0.32
$F(H\beta)$/ergs s^{-1} cm^{-2}	1.9 $\cdot 10^{-14}$
$F(H\alpha)$/ergs s^{-1} cm^{-2}	5.5 $\cdot 10^{-14}$

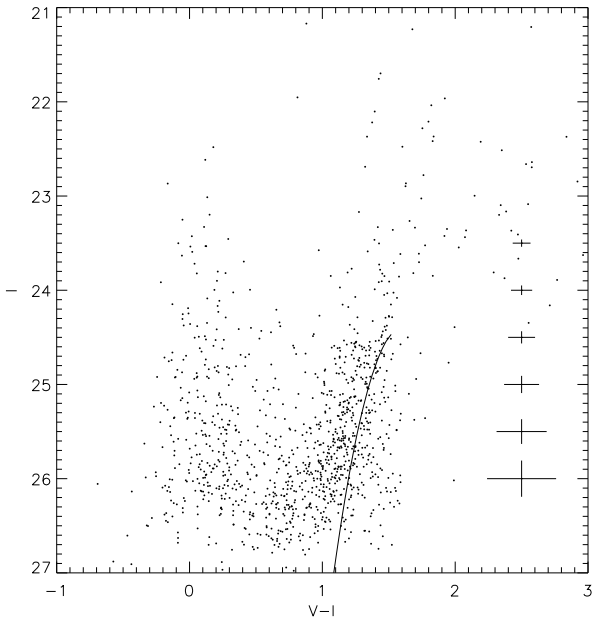

Figure 6. The $(V-I)$, I color magnitude diagram of HIPASS J1337-39. As a comparison, we have overlaid the fiducial RGB of the galactic globular cluster M 15 ([Fe/H]=−2.17). Photometric errors, obtained from the point spread function (PSF) fitting, are plotted on the right of the figure.

and OIII (see Table 2), allowing us to determine the oxygen abundance via the R_{23} indicator (Pagel et al. 1979; Skillman 1989) as 12 + log(O/H) = 7.25 ± 0.1, or [O/H] $\simeq$ 1/30 solar[4]. As a comparison, the abundance of I Zw 18 is 12 + log(O/H) = 7.2 (Izotov & Thuan 1999), therefore this galaxy appears to have a very low metal abundance. Using the relation between iron and oxygen abundances of Mateo (1998), we obtain [Fe/H]= -1.95 ± 0.2.

Since the metallicity is a measure of the degree of evolution of a system, the low abundance that we have derived suggests that J1337–39 is a poorly evolved system. To finally establish whether this is the consequence of an overall young age or not, we need to analyse the results of the resolved stellar photometry.

[4] Given the solar oxygen metallicity $\log(O/H)_\odot + 12 = 8.83$ (Grevese & Sauval 1998).

3.3 The morphology of the CMD

The CMD of J1337-39 is displayed in the left panel of Fig. 6. The right panel shows the CMD of the two remaining chips of the WFPC2 where the galaxy was not included that have been used to estimate the contamination of the field by foreground stars. The diagram clearly shows both a blue young stellar population with colours $V-I<0.7$, *the blue plume*, including main sequence (MS) and bright blue loop (BL) stars, and also a larger number of red stars at colours $0.7<V-I<1.5$ which clearly indicates the presence of a red giant branch (RGB) population. There is also evidence of a very narrow "red tail" elongated for roughly one magnitude above the tip of the RGB with colours $1.2<V-I<1.6$, which would suggest the presence of a metal-poor intermediate-age asymptotic giant branch (AGB) population. The evidence of a well-populated RGB here means that this galaxy must be at least older than 1 Gyr; HIPASS J1337–39 is *not* a *young* galaxy.

There are several age indicators in a CMD to set constraints on the age of the galaxy, but with this data set we can only detect stars which are roughly two magnitudes fainter than the tip of the RGB (TRGB), thus we are missing the oldest age indicators, such as the red clump and the horizontal branch stars. Intermediate age AGB and RGB stars are the oldest stellar population we can detect.

3.4 The RGB population

3.4.1 Deriving the distance to HIPASS J1337–39

The RGB can be seen as a high concentration of stars at $I>24.5$ and $0.7<V-I<1.5$. The absolute I-band magnitude of the tip of the RGB is not affected by metallicity and age variations (Iben & Renzini 1983), therefore it has been introduced as a robust distance indicator for resolved stellar systems (Da Costa & Armandroff 1990, Lee et al. 1993). To determine this parameter we have built the I luminosity function of stars with colours $0.7<(V-I)<1.7$ (Fig. 7). An edge detection Sobel filter (Madore & Freeman 1995) has been applied to the function. This produces a sharp peak when a sudden drop in the original function occurs, allowing the TRGB to be located. A cut-off in the RGB luminosity is found at $I_0 = 24.37 \pm 0.11$, where the magnitude has been corrected for the galactic extinction using $E_{B-V} = 0.07 \pm 0.01$ and $A_I = 1.85 \times E_{B-V} = 0.14 \pm 0.02$ (Schlegel et al. 1998). Assuming the TRGB to be $M_I = -4.05$, the distance modulus is $(m-M)_0 = 28.42 \pm 0.11$, giving a distance $D = 4.8 \pm 0.2$ Mpc. This value places J1337–39 in the region of M 83 (4.5 Mpc) although it is at a projected distance of 10° ($\sim$ 850 kpc at 4.8 Mpc) from the spiral.

3.4.2 A constraint on metallicity and age from the RGB

We can use the RGB to inspect the abundance of the red giant stars (the oldest population of stars that we can detect). The simplest method is to compare the colour of the RGB of this dwarf with that of well-known metal-poor galactic globular clusters (GGCs) (Da Costa & Armandroff 1990). In Fig. 6 the fiducial RGB of M 15, one of the most metal-poor GGCs with [Fe/H]= −2.17, is overlaid on the CMD of

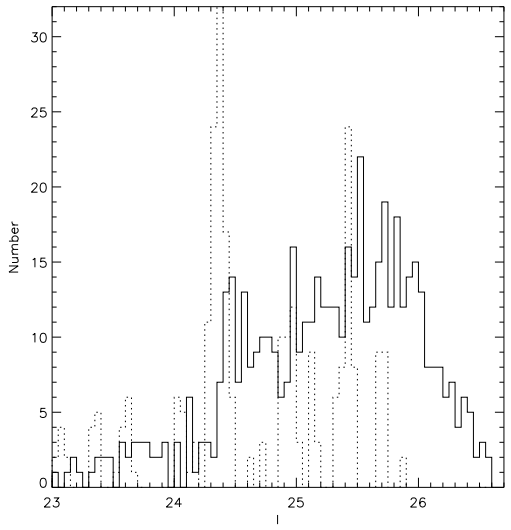

Figure 7. The luminosity function of the RGB of HIPASS J1337–39. The output of the edge detection Sobel filter is overlayed (dotted line). After having applied the filter we found the tip of the RGB at $I_0 = 24.37 \pm 0.11$.

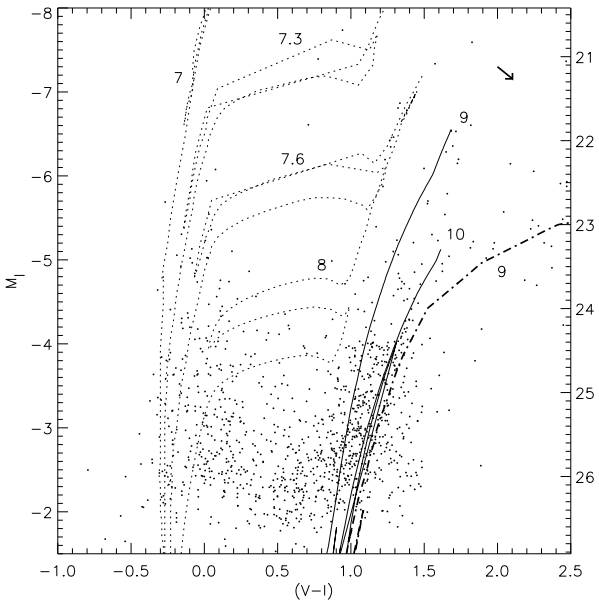

Figure 8. HIPASS J1337–39: dereddened $(V-I, I)$ colour magnitude diagram overlaid with Padua evolutionary tracks at Z= 0.0004 (*solid lines*) and Z = 0.001 (*dotted lines*). The different isochrones correspond to $\log(Age) = 7$ (10 Myr), 7.3 ($\sim$ 20 Myr) 7.6 ($\sim$ 40 Myr), 8 (150 Myr), 9 (1 Gyr) and 10 (10 Gyr). The dashed-dotted line indicates an isochrone at Z= 0.004 of age 1 Gyr, to show what is the maximum metallicity allowed to fit the colour of the RGB. The arrow at the top-right corner indicates the reddening vector.

J1337–39. Most of the RGB stars of J1337–39 extend blueward of the fiducial line representing the globular cluster, which suggests an even lower metallicity. We can estimate the metallicity of the stars in the RGB using the relation of Lee et al. (1993), even though this technique relies upon the hypothesis that the dominant population of the RGB is several Gyrs old (Population II stars). The mean of the distribution of the stars in the RGB gives a de-reddened colour at $M_{I,0} = -3.5$, $(V-I)_{-3.5} = 1.14 \pm 0.13$, which corresponds to an abundance [Fe/H]= -2.6 ± 0.6, placing it among the lowest metallicity nearby dwarf galaxies. The error on the photometry at that magnitude is rather large ($\Delta M = 0.15$) and produces a large uncertainty on the metallicity. Note also that Lee et al. relation in this case is used in extrapolation, since the least metallic globular cluster for which it has been determined is M 15 at [Fe/H]= -2.17. In any case, the comparison with M15 allows to infer that J1337-39 lies at the extreme metal poor end of dwarf galaxies and its abundance has to be lower than -2.17.

Such a low abundance is consistent with the value obtained from the optical spectroscopy if one assumes that the current generation of stars has been enriched with respect to the RGB population. We can also compare the CMD features with isochrones at different metallicities to definitely constrain the possible range of abundances and ages which can produce the observed colour of the RGB, while being at the same time consistent with the measured oxygen abundance.

Fig. 8 displays the stellar tracks from the Padua group (Bertelli et al 1994, Girardi et al. 2002). The set of isochrones which best fit the observed colour of the RGB is at Z = 0.0004 (1/50 solar). This abundance corresponds to a poor-metal scenario with an intermediate-age (1 - 10 Gyr) dominant stellar population. Fig. 8 also shows an isochrone of age 1 Gyr at Z = 0.004 (dashed line) demonstrating that at higher metallicity the bulk of the RGB stars would have to be younger than 1 Gyr, corresponding to a completely opposite scenario. This is the maximum metallicity allowed at which isochrones can match the position of the RGB in the diagram. However this possibility seems highly unlikely, since it would be difficult to explain a population of 1 Gyr old stars with a metallicity higher than the current abundance of the ISM.

Therefore, by comparing the colour and the shape of the RGB with the stellar evolutionary tracks we infer that the bulk of the red stars observed is a metal-poor population which is $\lesssim$ 10 Gyr old. Thus, the age of this dwarf galaxy appears consistent with formation in the early Universe rather than it being a recently formed system. Further evidence, supporting the low metallicity – intermediate-age population scenario will be discussed in the following sections, such as the presence of a low metallicity extended AGB branch.

3.5 AGB stars: tracing the intermediate-age population

The presence of low mass AGB stars in a galaxy is evidence for an intermediate-age population and thus that SF activity has taken place at look-back times of several Gyr. For this reason identifying AGB in these gas-rich dwarfs would set another constraint on their age and SF history. The distribution of intermediate-age AGB stars in the CMD depends very strongly on the metallicity: the higher the metallicity, the more extended this feature is towards colours redder than the RGB. At metallicities Z $\lesssim$ 0.001 the AGB extends

almost vertically above the RGB instead of bending towards redder colours (Cole et al. 1999).

Candidate AGB stars in J1337–39 form a very narrow "red tail" elongated for roughly one magnitude above the tip with colours similar to the RGB ($1.2 < V - I < 1.6$). This would suggest the presence of a metal-poor, intermediate-age AGB population. The isochrones at 10 Gyr and Z = 0.0004 (Fig. 8) match the thin red tail of AGB stars and define an approximate lower limit on the age of the galaxy. Using Z = 0.001 isochrones, the age of the AGB stars decreases to about 7 Gyr (not shown in the figure to avoid confusion). Therefore the AGB can be taken as a further argument in favour of the low-metallicity, intermediate-age scenario previously inferred from the RGB analysis.

We have also detected a number of very red stars at colours $V - I \gtrsim 2.0$ and brighter than the TRGB ($22 < I < 24.5$) whose nature is unclear. We have looked at the CMD of the adjacent fields to check if there are stars with similar photometric properties ($V - I > 1.9$, $22 < I < 24.5$) and find 15 such stars in the field, compared to 27 stars detected around J1337–39. The probable contamination by foreground stars in the area is lower than the number of stars observed ($N_{obs} - N_{foreground} = 12 \pm 6$), thus we can not exclude that they may belong to the dwarf.

However, after having verified that they are point-source like in appearance, we have checked their position in the galaxy and compared their distribution to the other candidate AGB stars at bluer colours forming the narrow red tail above the TRGB. The redder AGB stars are mostly found at the border of the main body of the galaxy, with a wider distribution than the bluer AGB candidates.

The presence of these stars in HIPASS J1337–39 is a puzzle. If they are AGB stars then their red colours are not easy to explain and they imply the presence of a higher metallicity population. Only isochrones of age between ~ 1 and 3 Gyr at Z = 0.004, in fact, can match their location on the CMD (Fig. 8), but this would be in sharp contrast with the lower abundance of the ISM that we have measured. If they belong to HIPASS J1337–39, they would be younger than the bluer (and lower metallicity) AGB candidate stars. If this were the case, how can they more widely spread throughout the frame than the older AGB stars, mostly detected within or around the optical body of the galaxy?

Without further observations, either spectroscopy or narrow band photometry using the $Ti - O$, or CN filters it is not possible to discriminate the nature of these red stars in J1337–39 and to understand if they belong to the dwarf galaxy rather than being foreground galactic stars.

To summarise, it appears from the red features in the CMD of J1337–39, that the galaxy contains a dominant population which is at least several Gyr old, with a lower limit on the age set by the presence of candidate AGB stars. From the comparison with isochrones that fit the position of the AGB stars, one obtains at Z = 0.0004 an upper limit of $\sim$ 10 Gyr (or $\sim$ 7 Gyr if the metallicity of the isochrones is Z = 0.001). The possible presence of a population of very red AGB stars in HIPASS J1337–39 does not fit very well with the scenario of a galaxy with an overall low metal abundance and remains a puzzle.

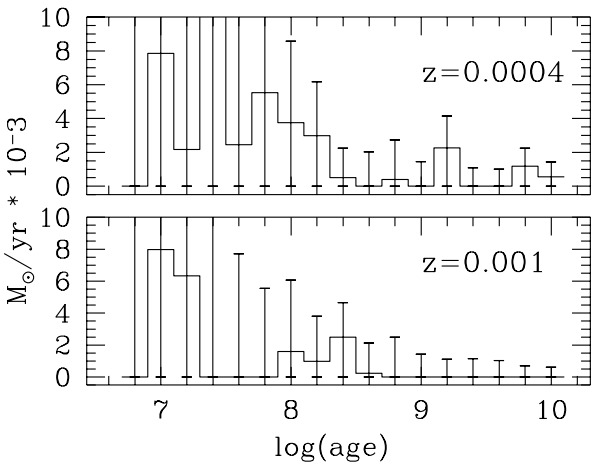

Figure 9. The SFH of J1337–39 obtained with a combination of stellar isochrones with metallicities Z = 0.0004 and Z = 0.001. We find two main episodes of star formation: one between 6 and 10 Gyr (log(*Age*) =9.8 - 10), and the other around 1.5 Gyr (log(*Age*) =9.2). An increase in the SFR seems to occur in the last 200 Myr.

3.6 The recent SFH

The evidence of recent star formation activity in HIPASS J1337–39 is clearly inferred from the population of young and blue stars at colours $V - I \lesssim 0.5$ extending up to $I \simeq 22$ (Fig. 8). This "blue plume" is populated by intermediate mass stars in the main sequence (MS) phase and more evolved core helium burning stars of the blue loop (BL) that form a redder track parallel to the MS. The location of the different evolutionary stages is shown by the isochrones at Z = 0.001 (*dotted line*) in Fig. 8. We used a higher metallicity set of isochrones for the recent stellar population to be consistent with the results from the HII region analysis. There is evidence for fairly continuous star formation activity between 20 and 100 Myr. In fact the bright red supergiant stars with an absolute magnitude $-6 > M_I > -7$ are fitted by the isochrone at log(*Age*) = 8 and 7.6, while the positions of the brightest blue supergiants in the diagram are consistent with isochrones around 20 (log(*Age*) = 7.3) and 40 Myr log(*Age*) = 7.6. The stars in the MS appear to be no older than 10 Myr.

3.7 Modelling the SFH of HIPASS J1337–39

We have used the STARFISH package of Harris & Zaritsky (2001) to investigate the SFH of the galaxy. First a linear combination of synthetic CMDs is built by a set of stellar isochrones, taking into account the scatter in the stars' photometry as follows from artificial star tests (see §2.2 for details), the interstellar extinction and the distance modulus of the observational data. Then the code compares the synthetic and the observed CMDs. It determines the best-fit SFH performing χ^2 minimization of the differences in the number of stars between the model and the data in the different regions of the diagram.

We used the set of isochrones provided by the Padua group with different values of the metallicity. We considered

Table 3. The list of the different combination of metallicities inspected with STARFISH and the corresponding reduced χ^2 parameter. For HIPASS J1337-39 we find that the best-fit SFH is given by a model with isochrones at Z = 0.0004 and 0.001.

Z	χ^2
0.0004	1.25
0.001	1.33
0.004	1.34
0.0004+0.001	1.08
0.001+0.004	1.28
0.0004+0.001+0.004	1.13

the entire range of available ages (from 10^7 yr to $10^{10.2}$ yr) with a step of $\log(Age) = 0.2$. We adopted a Salpeter initial mass function(IMF), a binary fraction of 0.5, and we included Galactic foreground extinction (but not any internal extinction in the dwarfs).

For HIPASS J1337-39 the distance modulus was set to $(m - M)_0 = 28.42$. The metallicity is constrained between 1/50th and 1/30th solar from the analysis of the CMD and the oxygen abundance. Therefore we have created synthetic CMDs with various combination of isochrones at Z = 0.0004, Z = 0.001 and also at Z = 0.004 to test the effects of a higher metallicity component. In Table 3 we show the fits we obtained for different metal abundances.

The resulting SFH (Fig. 9) which gave the lowest reduced χ^2 value and the best agreement between the observed and synthetic CMDs corresponds to the combination of the isochrones at Z = 0.0004 and Z = 0.001. From the figure there is evidence of an extended period of SF around 6 - 10 Gyr ($\log(Age) = 9.8$, 10) for Z = 0.0004. The galaxy then appears to go through a rather quiescent period until about 1.5 Gyr ago. For ages around or less than 1 Gyr the SFR seems to be rather low except for the remarkable enhancement in the last 200 - 250 Myr. The oldest stars have metallicities Z = 0.0004, while populations with higher metal abundance appear only in the last Gyr.

The error bars are determined by the code identifying the 68% (1σ) confidence interval on each amplitude. The number of stars in the diagram is low, especially the young blue ones, which makes the statistical analysis and modelling extremely difficult in this part of the diagram. For this reason the uncertainties in the SFR estimation are rather large at recent epochs.

The corresponding model CMD is displayed in Fig. 10 and compared to the observed data. The two diagrams look fairly similar. The average colour of the simulated RGB is consistent with the observed one. The main differences appear in the modelling of the red stars above the tip of the RGB. A few intermediate-age AGB stars are found in the two oldest age bins ($\log(Age) = 9.8$, 10) but they are not distributed as a narrow plume just above the TRGB as in the data. Moreover too many red bright stars with $22 < I < 24$ and colours $1.2 < V - I < 1.7$ appear in the age bin corresponding to $\log(Age) = 9.2$, indicating that the SFR in that bin has been overestimated by the code.

A model CMD built using only the highest allowed metallicity, Z = 0.004 fails to reproduce the observed diagram and the corresponding fit has a higher χ^2 value.

To conclude, the simulation of the SFH of HIPASS J1337–39 points toward a scenario with a low metallicity population with an age as old as 10 Gyr, in agreement with our analysis of the CMD.

3.8 Summary and discussion

Our results show that HIPASS J1337–39 is not a young galaxy. To explain the colour of the RGB with a population of young stars would require a metallicity of around 1/5 solar (Z = 0.004), which would be inconsistent with the metal abundance measured in the ISM. On the other hand, comparison of the CMD with theoretical low-metallicity isochrones indicates that the RGB may contain stars as old as 10 Gyr. The detection of AGB stars gives further evidence that the galaxy may harbour an intermediate-age stellar population.

The synthetic CMD is able to reproduce the main features of the observed one. Again, this implies that the first episode of SF occurred $10^{10\pm0.1}$ years ago. We find an average SFR over 10 Gyr of $\sim 2 \times 10^{-3}$ $M_\odot$ yr^{-1}, and the SFH of J1337–39 appears to be characterised by three main episodes of SF (between 6 and 10 Gyr, around 2.5 Gyr and in the last 250 Myr).

Nevertheless, to firmly prove the existence of an old stellar component one should unearth a population of horizontal branch (HB) stars, which would require much deeper observations with the HST.

If our interpretation is correct and this galaxy harbours a stellar population older than a few Gyr, the low oxygen abundance that we have measured is remarkable as it indicates that the galaxy has undergone little chemical enrichment during its evolution.

We have also analysed the neutral gas content of J1337–39 to investigate its distribution and its relation with the SF activity. The galaxy has an overall HI column density which is above 10^{20} cm^{-2} until 2 kpc from the centre. The HI peak density (few times 10^{21} cm^{-2}) coincides with the area where the HII regions are found. The HI distribution around J1337–39 appears regular overall, apart from an unexplained "tail" to the north west.

There do not seem to be any objects within the 30′ field of view of the ATCA telescope to explain the slightly disturbed HI morphology as the effect of a tidal interaction with a close companion. Moreover, at the distance of 4.8 Mpc that we derived from the tip of the RGB, J1337–39 seems to be located on the margins of the Centaurus A group. The galaxy is about 10°(∼ 850 kpc) from M83, the closest large galaxy in the Centaurus A group. Among the other massive galaxies of the group, NGC 5102 is at a radial distance d = 3.4 Mpc, while NGC 5253 is at $d = 3.9$ Mpc (Karachentsev et al. 2002) at an angular separation of about 8 degrees – both of these are well over 1 Mpc from J1337–39.

The shape of the HI distribution could be due to the interaction with a hot intracluster medium. A galaxy moving with a velocity v_G through a hot diffused gas is subjected to a ram pressure given by $p_{ram} = \rho_{ICM} v_G^2$, where ρ_{ICM} is the density of the medium. However this seems unlikely as the hot gas density should be lower at the edge of the group and J1337–39 is one of the most distant dwarfs from M83.

J1337-39 is at only 4 degrees in projection from NGC 5128, which is the nearest active galactic nucleus. NGC 5128

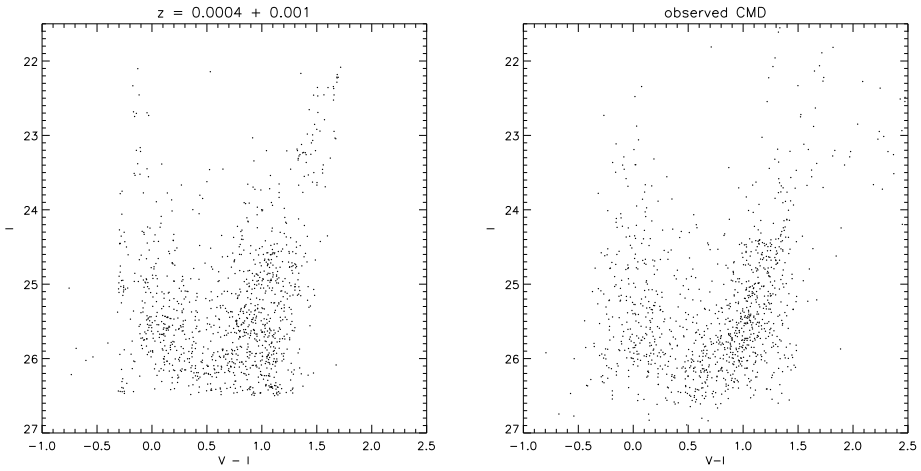

Figure 10. The comparison between the model *(left)* and the observed CMD of HIPASS J1337–39 *(right)*.

shows both large radio lobes covering at 1410 MHz an area of $8^\circ \times 4^\circ$ in the north south direction (Cooper et al. 1965; Junkes et al. 1993), and extended X-ray emission ($7^\circ \times 1.5^\circ$) along the direction north east - south west, rotated about 50 degrees from the axis of the radio lobes (Arp 1994). The region of X-ray emission around Cen A corresponds to roughly 400 kpc, and indicates the existence of a diffuse hot gas ($\sim 10^7$ K) (Arp 1994). From the Rosat map, this emission would include the area of the sky where J1337-39 is found. However the relative distance between the two galaxies is about 1.4 Mpc, assuming that $d_{CenA} = 3.66$ Mpc and $d_{39} = 4.8$ Mpc. Without any indication on the effective direction of the X-ray jet with respect to J1337-39, and given the large relative distance between the two galxies is difficult to argue that the HI morphology of this dwarf is an indication of ram pressure stripping interaction with NGC 5128.

Alternatively, the HI distribution may be the result of a recent accretion of gas which would be consistent with the irregularities in the velocity field in the HI tail. The possible accretion of an HI cloud may be related to the apparent increase in the SF activity around 100 Myr ago that was inferred from the analysis of the model and observed CMDs. Higher resolution HI data are needed to investigate the structure of the gas distribution in J1337–39 in more detail.

4 HIDEEP J1337–3320

HIDEEP J1337–3320, which was found in a deeper HI survey than the other dwarfs, has the lowest HI mass, $M_{HI} = 5 \times 10^6$, and column density (see Table 1). Its gas fraction is also lower than the others ($M_{HI}/L_B = 1.4$ in solar units). Optically, we find a small and rather compact object with no evidence for ongoing star formation. We are therefore unable to independently constrain the metallicity by measuring the oxygen abundance, and thus are faced with difficulties in the analysis of the CMD due to the age-metallicity degeneracy.

4.1 The neutral gas content

HIDEEP J1337–3320 has a very smooth HI distribution that is centred on the stellar component of the galaxy (Fig. 11), although the presence of local clumps and perturbations could be smeared out by the large beam size, which only marginally resolves the galaxy. The neutral gas extends beyond the optical counterpart out to $45''$, ~ 1 kpc at an assumed distance of 4.4 Mpc (see below), and can be traced out to a column density $N_{HI} = 5 \times 10^{19}$ cm^{-2} . The gas density around the stellar distribution is almost constant, but yet it is low, hovering around $N_{HI} = 2 \times 10^{20}$ cm^{-2} with a central peak at $N_{HI} = 2.3 \times 10^{20}$ cm^{-2} . In general dIrr star forming galaxies in the LG show more asymmetric HI distributions with holes and arcs as in IC 10 (Wilcots & Miller 1998) or SagDIG (Young & Lo 1997) that may be created by supernovae or stellar winds. The smooth distribution of the gas may give hints of a lack of star formation in the last ~ 100 Myr, however, one has to keep in mind that the low resolution of the observations may have smeared out irregularities in the HI structure. There is some evidence of a velocity gradient both from the velocity contours (Fig. 11, right panel) and from the individual channel images (not shown here).

The HI profile is centred at 592.1 $\pm$ 0.8 km s^{-1}, with a 20% velocity width $\Delta v_{20} = 38$ km s^{-1}and a velocity dispersion $\sigma_v \simeq 8$ km s^{-1}. We derive an HI mass of $M_{HI} = 5.1 \times 10^6\ M_\odot$, at a TRGB distance of 4.4 Mpc (see below). The dynamical mass, without any inclination angle correction, is $M_{dyn} \simeq 8 \times 10^7\ M_\odot$, giving $M_{HI}/M_{dyn} \simeq 0.06$.

4.2 Optical properties

The optical image of HIDEEP J1337-3320 (Fig. 12) shows a smaller and more compact object than J1337-39. It does not seem to have signs of ongoing star formation activity and the WIYN snapshots did not show evidence for HII regions. The stellar distribution looks very smooth and regular, and its surface-brightness distribution can be fitted by an exponential profile.

Its optical morphology and the presence of gas

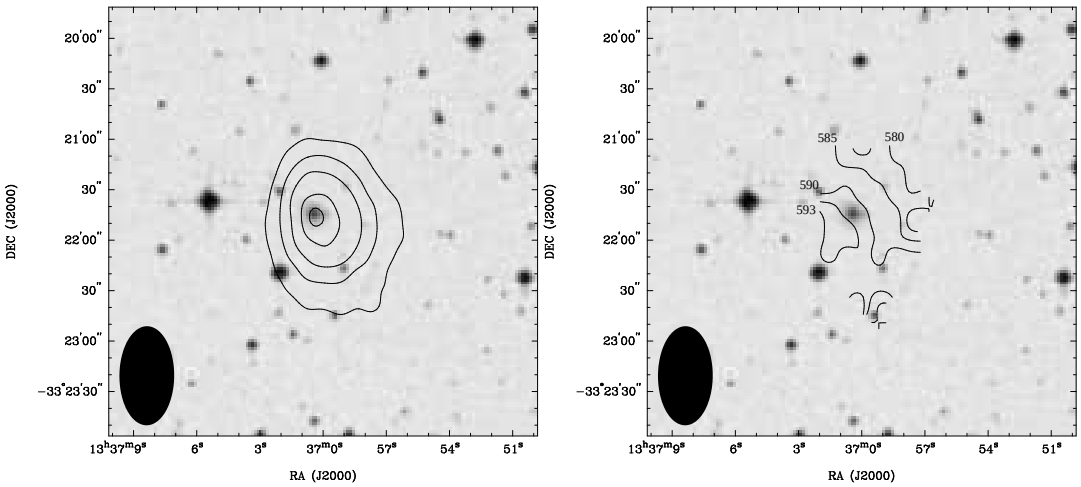

Figure 11. *Left:* HI density contours overlaid on the DSS field including the galaxy. The contour levels are: 0.5, 1.0, 1.5, 2.0, 2.25 $\times 10^{20}$ cm^{-2} . *Right:* The velocity field displayed in the range v = 580 km s^{-1}and v = 593 km s^{-1}. The beam size is shown at the bottom left corner of the image.

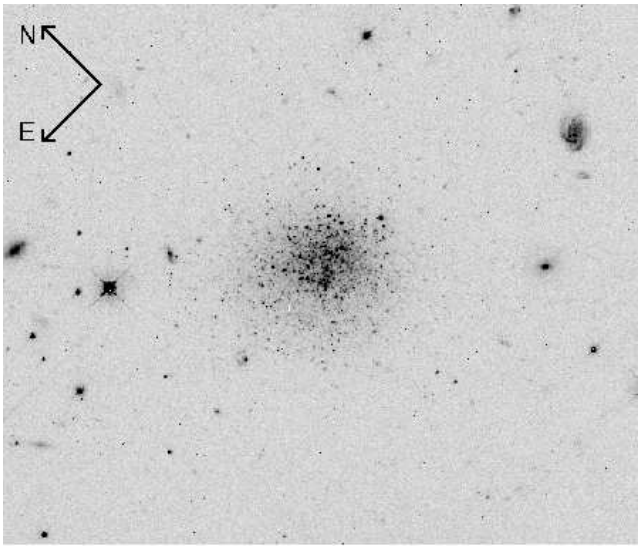

Figure 12. The WFPC2 image of HIDEEP J1337–3320 taken with the filter F555W. The size of the frame is roughly 80″.

(M_{HI}/L_B = 1.4) resemble the transition type dwarfs of the Local Group such as LGS 3, Phoenix, and DDO 210 (although they have much lower M_{HI}/L_B ratios) and the more gas-rich dwarfs with intermediate properties between dSphs and dIrrs found by Skillmann, Côté & Miller (2003, hereafter SCM03) in the Sculptor group.

4.3 The morphology of the CMD

In the left panel of Fig. 13 the (I, $V-I$) morphology of the CMD is shown. The main features at red colours are a narrow RGB, a few candidate AGB stars, some of them with colour $(V-I) > 2$. The blue part of the diagram, on the other hand, is less populated, especially if compared to J1337-39, and from the comparison with theoretical isochrones (see section 4.6) it seems to contain mostly blue loop stars, suggesting no SF activity within the last 10 - 30 Myrs.

4.4 The RGB, and the distance to HIDEEP J1337-3320

The RGB is the most prominent feature of the CMD. It is slightly redder than that of J1337-39 and is located between $V-I = 1$ and $V-I = 1.6$. As with J1337–39, the distance to the dwarf can be determined from the I magnitude of the tip of the RGB. This is found at $I_0 = 24.15 \pm 0.10$ (Fig. 14) assuming a galactic reddening $E_{B-V} = 0.049 \pm 0.008$ and $A_I = 0.10 \pm 0.01$. The dereddened distance modulus is $(m-M)_0 = 28.20 \pm 0.10$ and the resulting distance to HIDEEP J1337-3320 is $D = 4.4 \pm 0.2$ Mpc.

At an angular separation of about 3.5° from M 83 ($\lesssim$ 300 kpc at 4.5 Mpc) and a comparable radial distance (d_{M83} = 4.5 Mpc) HIDEEP J1337-3320 seems to be located in a position within the group that is much closer to the massive spiral than J1337-39.

In Fig. 13 we have overlayed on the CMD of J1337-3320 the RGB of the galactic globular cluster M 15, suitably scaled to the distance of 4.4 Mpc. The colour of the RGB of M 15, with a metallicity [Fe/H]= −2.17, is slightly bluer than the mean distribution of the observed RGB. Therefore, if we assume that the galaxy has a population of stars which is at a few Gyr old, we can obtain a lower limit on the average abundance of J1337-3320. Using the method of Lee et al. (1993) to estimate the metallicity from the colour of the RGB, we find [Fe/H]= -1.9 ± 0.6, slightly higher than HIPASS J1337-39.

When the CMD is compared with Padua stellar evolutionary tracks, we find that the Z = 0.001 set provides the best fit to the RGB. In this scenario, the population of the RGB appears to be as old as 10 Gyr. However, a different choice of the metallicity changes the upper limit on the age one can derive from the RGB. If we use the Z = 0.004 (1/5 solar) isochrones, as shown in Fig. 15, the oldest track which matches the RGB is at about 4 Gyr. Tracks with ages around and older than 1 Gyr can also fit the position of the very red stars (possible AGB candidates) at $V-I > 2$. In this scenario, the blue part of the RGB (i.e. stars with $1 < V-I < 1.6$ and $I > 24.2$) would be very young, with an age between 250 Myr and 1 Gyr, as one can see from

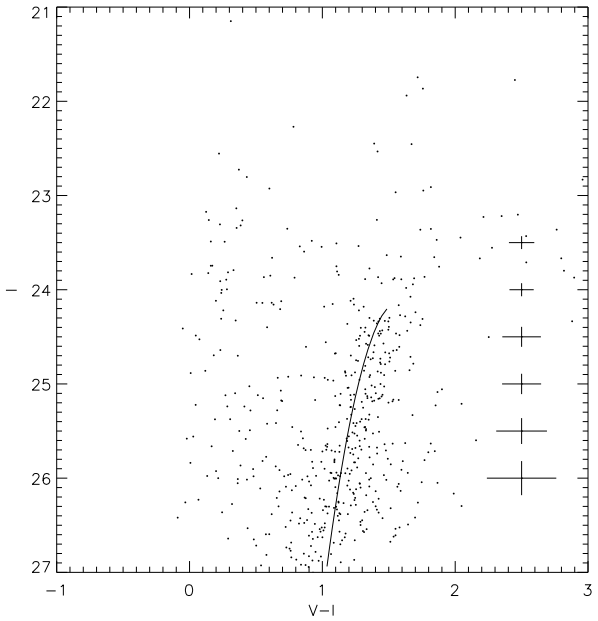

Figure 13. HIDEEP J1337-3320: $(V - I)$, I color magnitude diagram. The solid line correspond to the RGB of the galactic globular cluster M 15 and its location shows that the metallicity of J1337–3320 is on average slightly higher than M 15 ([Fe/H]= −2.1).

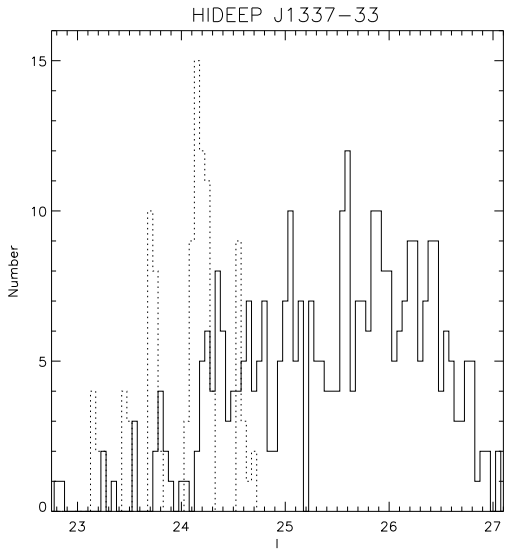

Figure 14. The I luminosity functions of HIDEEP J1337–3320. The dotted line represents the output of the edge detection filter used to detect the tip. The peak indicates the position of the tip which has been found at $I_0 = 24.15 \pm 0.1$

the right panel of Fig. 15. The age of the onset of the helium flash is between 0.9 and 1.5 Gyr, therefore the stars with Z = 0.004 and ages $\lesssim$ 1 Gyr would be ascending the AGB for the first time, rather than being in the red giant phase. However AGB stars do not show a clear-cut cutoff in luminosity as RGB stars do, thus, in this scenario, a sharp decrease in the number of stars at $I \sim 24.2$, i.e. the tip of the RGB, would probably not be detectable in the diagram - as it clearly is.

The shape of the red branch and the presence of a clear cut-off in the luminosity function around $I \sim 24.2$ can be taken as evidence of the existence of an intermediate-age population of red giants. A similar argument has been used in other systems (such as Leo A; Tolstoy et al. 1998) when more reliable age indicator have not been detected in the CMD.

4.5 The AGB

A small number of objects, potentially AGB stars, have been found above the TRGB (Fig. 13), some of them (24 ± 5) with the very red colours $(V - I > 1.7)$ we found in J1337-39. If these stars belong to J1337–3320, then they should have a metallicity greater then 1/20 solar (Z=0.001), at which, according to synthetic models, the AGB branch starts bending horizontally towards the reddest part of the diagram (Fig. 15), revealing the presence of a more metal-rich population in the galaxy. The local contamination around $V - I > 1.7$, appears to be low. Indeed in the adjacent fields of the camera where the galaxy was not included (WF2 and WF4), we have detected 11 ± 3 stars with $V - I > 1.7$ and $22 < I < 25$.

Most of the candidate AGB stars are found within or around the main optical body of the dwarf. Some of the reddest stars, however, are clearly outside the bulk of the stellar distribution. They are likely to be foreground stars, but we cannot exclude that they belong to the dwarf since there are examples in the LG galaxies, such as IC 1613 (Albert, Demers, & Kunkel 2000), DDO 210 and Pegasus (Battinelli & Demers 2000), Leo I (Demers & Battinelli 2002) where Carbon stars extend even further out than the observed HI content.

It is possible that there is a population of old AGB stars with colours similar to that of the TRGB whose position on the CMD is fitted by the same low metallicity isochrones (Z = 0.001) as the RGB. However, only isochrones at Z = 0.004 (1/5 solar) can fully match their position on the diagram, thus it could be that we have found a population of very red and bright AGB stars formed at a later epoch with a higher metallicity. The very red AGB population may give a hint of the chemical evolution of the galaxy through its different episodes of star formation. The isochrones at Z = 0.004 also match the position of the fainter and bluer AGB stars, thus we cannot be certain that there is only a single population of relatively young and metal-rich AGB stars. Therefore spectra or narrow-band photometry are needed to measure their metallicity in order to improve our understanding of the reddest stars in J1337-3320.

4.6 The younger stellar populations.

The blue plume of HIDEEP J1337-3320 (Fig. 13) is much less populated than that of J1337-39. There are few bright stars up to $I \sim 22.5$, which is likely to be the bluest extent of the helium burning phase from comparison with the theoretical isochrones (Fig. 15). A well defined main sequence though is lacking which implies a drop of the recent SF activity.

Isochrones at Z = 0.001 fitting the magnitudes and colour of the brightest blue loop stars indicate that the age

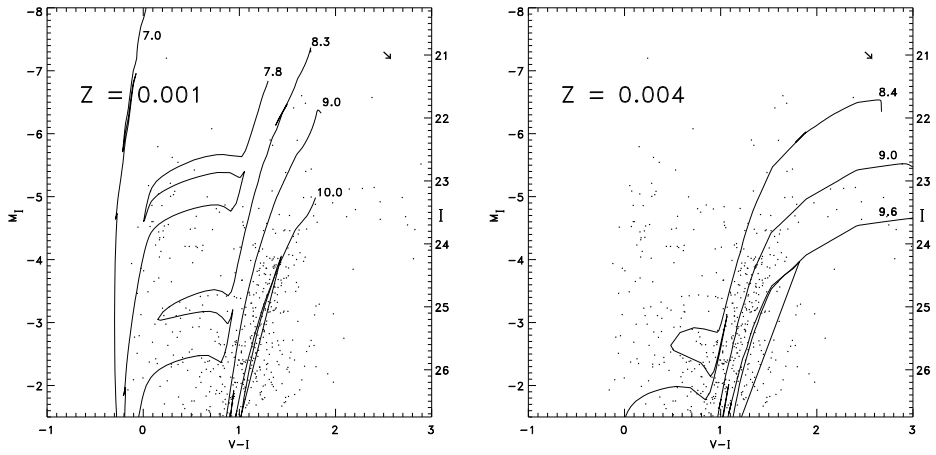

Figure 15. HIDEEP J1337-3320: dereddened $(V-I)$, I color magnitude diagrams overlaid with isochrones at Z = 0.001 *(left)* and Z = 0.004 *(right)*. According to the metallicity used, the limit one can set on the age of the red giant population changes from 10 to 4 Gyr. At Z = 0.004, the blue part of the feature that we define as the RGB (i.e. stars with colours between 1 and 1.6 and luminosity fainter than $I = 24.2$) would be younger, with an age between 250 Myr and 1 Gyr, therefore it would be mostly populated by AGB stars rather than red giants. The age of the younger blue stellar population, which are mainly core helium burning stars is shown in the left panel. Blue and very young main sequence stars (age less than 10 Myr) seems to be lacking. The arrows at the top-right corners indicate the reddening vector.

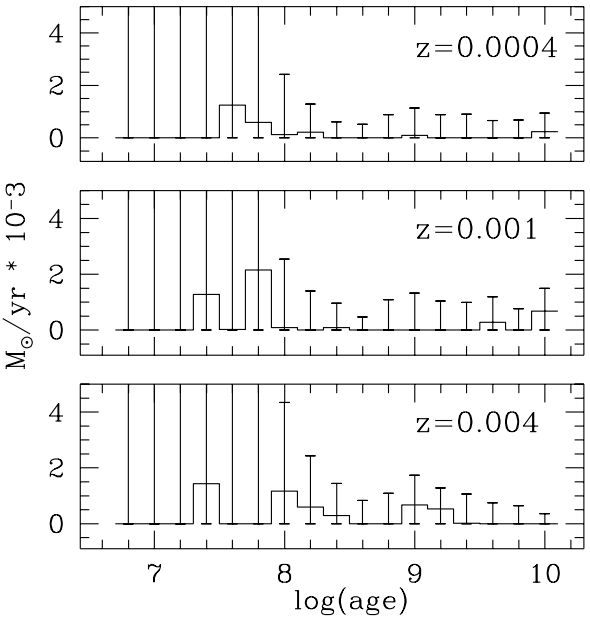

Figure 16. The best fit SFH of J1337-3320.

of the most recent stars in this galaxy is around 60 – 100 Myr, when the last episode of significant SF activity probably occurred.

4.7 SFH of HIDEEP J1337-3320

We have used STARFISH to model the SFH of J1337-3320. The different combination of metallicities inspected and the corresponding reduced χ^2 values are shown in Table 4. The best-fit SFH and the model CMD are displayed in Fig. 16 and in the left panel of Fig. 17 respectively. The observed CMD is also shown in the right panel of Fig. 17 for comparison with the synthetic diagram. The best fit is the result of the combination of three sets of isochrones, Z = 0.0004, Z = 0.001, and Z = 0.004.

Table 4. The list of the different combination of metallicities inspected with STARFISH and the corresponding reduced χ^2 parameter. For HIDEEP J1337-3320 we find that the best-fit SFH is given by a model with isochrones at Z = 0.0004, 0.001 and 0.004.

Z	χ^2
0.0004	1.47
0.001	1.22
0.004	1.36
0.0004+0.001	1.26
0.001+0.004	1.23
0.0004+0.001+0.004	1.15

The evolution of J1337-3320 seems to be dominated by an early SF event at $10^{+2.5}_{-2.0}$ Gyr where the majority of the red giant stars have been formed. After this episode the galaxy appears to have experienced episodes of SF occurring around 4 Gyr and 1 – 1.5 Gyr followed by periods of apparent inactivity. SF seems to be triggered again around 250 Myr with an increased SFR until around 25 Myr, peaking between 60 and 100 Myr. At ages younger than 100 Myr the errors in the SFR become very large, affecting the results of the model for the youngest stars.

The overall SFR appears to be very low, and it never exceeds 2×10^{-3} $M_\odot$ yr^{-1}. There is a degeneracy at 10 Gyr between the isochrones at Z = 0.0004 and Z = 0.001. Syn-

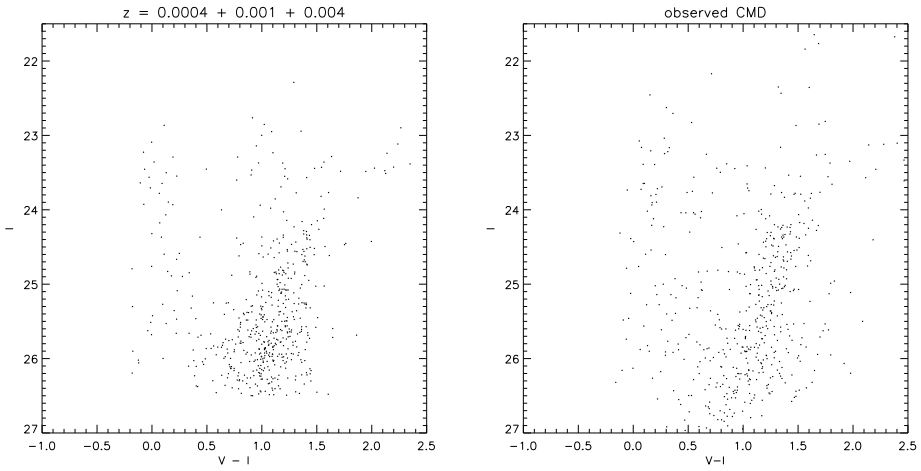

Figure 17. The best fit model CMD (*left*) compared to the observed one (*right*). We find a good agreement between the two diagrams although there is an overestimate of the old SFR which produces a more populated RGB at faint magnitudes.

thetic CMDs with Z = 0.0004 and Z = 0.001 are photometrically too similar for the method to be able to distinguish between them with the current data. We observe a consistent age-metallicity relation in the SFH. The oldest stars have Z = 0.0004/0.001 while there is no significant population with Z = 0.004 before log (Age) = 9.2 which suggests a gradual metal enrichment due to the previous SF episodes.

The model CMD reasonably matches the main features of the observed one. The main difference found is in the width of the RGB, which is too large at faint magnitudes in the model, probably due to an overestimate of the SFR in the 10 Gyr age bin. From our simulation, the majority of the red giant stars appear in the 10 Gyr interval. On the other hand, the recent SFR seems to be slightly underestimated, with a small difference in the number of young stars between the model and the data. The synthetic CMD also show a red tail of stars above the TRGB extending at colours $(V - I) > 1.5$, which appears at $\log(Age) = 9$, 9.2 with a higher metallicity (Z = 0.004).

To conclude, the evolution of J1337-3320 seems to be characterised by periods of low SF activity followed by quiescence (the so called "gasping" evolution). The average SFR is always below 2×10^{-3} $M_\odot$ yr^{-1}. At more recent epochs, we find an increase in the SF activity within the last 200 Myr, with a peak around 60 - 100 Myr, but there is no evidence of young stars with ages less than 10 Myr.

4.8 Summary and discussion

Despite the significant amount of neutral hydrogen compared to its stellar mass, there is no evidence of ionised gas in HIDEEP J1337-3320 to constrain the current abundance of the ISM, as was possible with HIPASS J1337-39. Therefore the age and the metallicity evolution of this galaxy must be estimated using only the CMD.

We find a dominant population of red giants which, from the shape of the RGB, comparison with the stellar tracks, and the distribution of the stars, appears to be of at least intermediate age. J1337–3320 *seems not* to be a *young* galaxy, but rather has experienced star formation activity over the last 10 Gyr. This scenario is consistent with the STARFISH modelling. The observed large gas fraction appears to be the result of a very low SFR, which never exceeds 2×10^{-3} $M_\odot$ yr^{-1}. After the main event at $10^{+2.5}_{-2.0}$ Gyr when most of the red giant stars in the galaxy are formed (according to our model CMD), the subsequent evolution seems to be characterised by smooth episodes of SF activity and periods of quiescence.

From the colour of the red giant branch we have obtained a measure of the metallicity of the intermediate-age population, and we find [Fe/H] $= -1.9 \pm 0.6$ which indicates a very low metal content. The synthetic CMD built with low metallicity isochrones are compatible with that value, but the best-fit SFHis is given by the combination of three sets of isochrones (Z = 1/50, Z = 1/20, Z = 1/5 of the solar abundance), which would give indication of chemical enrichment throughout the evolution of this dwarf.

An estimate of the metal content can also be inferred from the metallicity luminosity relation (Skillman et al. 1989, Richer & McCall 1995, hereafter RM95). Following RM95 we derive that 12+ log(O/H) = 7.2 ± 0.2, where the error is given by the uncertainty on the coefficients in the relation of RM95. This corresponds to a metallicity in the range between 1/70 and 1/30 of the solar value (with [Fe/O] = 0). The metal content of the recent stellar population derived from the model SFH ranges between Z = 0.001 (1/20 solar) and Z = 0.004 (1/5 solar) (Fig. 16), thus with these values the galaxy would stand out in the luminosity-metallicity relation.

To conclude, the general properties of J1337-3320, such as the low luminosity, the spherical symmetry of the optical appearance, and the absence of current SF activity despite the large gas reservoir, make this dwarf similar to the so called "transition objects" of the LG (e.g. DDO 210, LGS 3 and Phoenix), which show intermediate properties between dIrrs and dSphs. These systems are preferentially found nearer than dIrrs (but not as close as dSphs) to the most massive members of a group and are generally interpreted as dIrr galaxies going through a period of temporary interruption of their star formation activity.

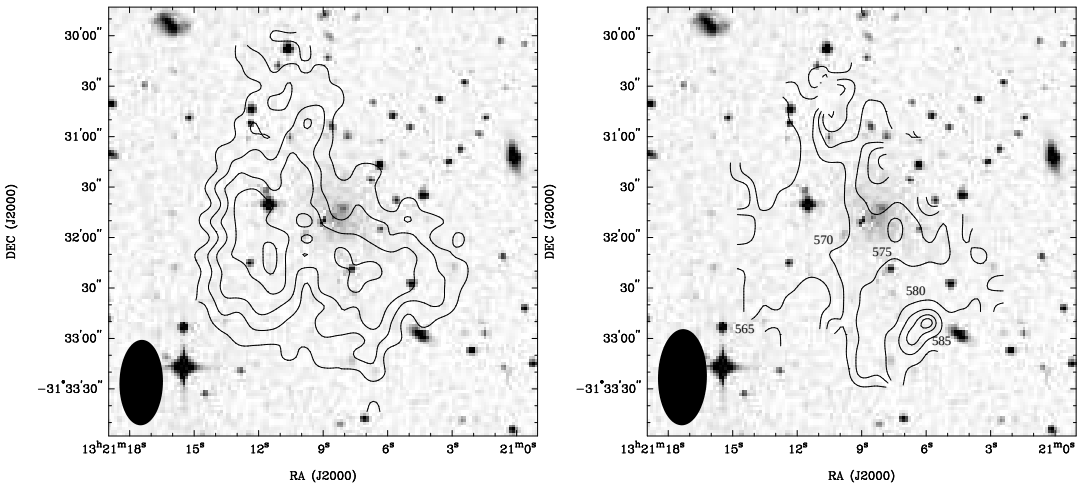

Figure 18. HIPASS J1321-31: *Left:* HI contour density maps overlaid on the DSS image of the galaxy. The contour levels are: 0.5, 1.0, 1.5, 2.0, 2.25, 2.35 $\times 10^{20}$ cm^{-2} . *Right:* The HI velocity field. There is evidence of a gradient in the velocity field, but it is difficult to infer from this map clear evidence of organized rotation. The beam size is shown at the bottom left corner of the image.

5 HIPASS J1321–31

HIPASS J1321-31 is the most puzzling object among the three. With a mass of $M_{HI} \simeq 4 \times 10^7$ $M_\odot$ and an apparent magnitude $m_B = 17.1 \pm 0.2$ mag (Banks et al. 1999), it has the highest gas-mass-to-stellar light ratio ($M_{HI}/L_B \simeq 5$), yet Hα snapshots taken with the WIYN telescope do not reveal any HII regions. It is also the galaxy with the lowest SB among the three dwarfs: Banks et al. (1999) found $\mu_0^B = 24.2$ mag arcsec^{-2}. It appears to be located in the region surrounding M 83, but its CMD is markedly different from the other dwarfs in our sample, showing that it has undergone a different SFH (Pritzl et al. 2003, hereafter Pr03).

5.1 The neutral gas content

The HI distribution of HIPASS J1321-31 (Fig. 18) extends out to a radius of 1′30″ (2.3 kpc at the distance of 5.2 Mpc from the TRGB derived in Pr03) and is clearly offset from the optical centre. There are two peaks in the HI density but they fall near the edge of the chip where the galaxy is located (WF3), showing poor correlation with the main optical counterpart. The column density is low overall and peaks at only 2.5×10^{20} cm^{-2}.

A small gradient in the velocity map can be seen in Fig. 18, but generally the velocity field seems rather disturbed. It is difficult to infer evidence of rotation from the contours, however it appears a variation in the kinematics between the south-western and north-eastern regions of the galaxy.

The HI profile is centred at 579 ± 1 km s^{-1}, with a 20% velocity width $\Delta v_{20} = 59$ km s^{-1}and a velocity dispersion $\sigma_v \simeq 8$ km s^{-1}. We derive a total HI mass of $M_{HI} = 3.7 \times 10^7$ $M_\odot$ (at a radial distance d = 5.2 ± 0.3 Mpc).

The dynamical mass, without any inclination angle correction, is found to be $M_{dyn} = 7 \times 10^8$ $M_\odot$, giving $M_{HI}/M_{dyn} \simeq 0.05$. We have looked through the ATCA cube to inspect the local environment of the dwarf. There is no sign of HI clouds or other low mass gas-rich objects in the 30′× 30′field of view up to our column density limit of $N_{HI} = 5 \times 10^{19}$ cm^{-2} .

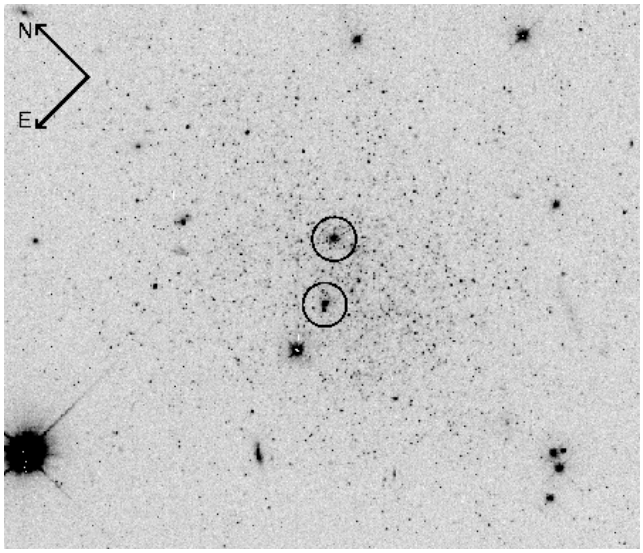

Figure 19. WFPC2 image in the F555W filter of HIPASS J1321-31. The two circles show the candidate "fading" HII regions in the galaxy. The size of the field is approximately 80″.

5.2 The optical properties

Optical observations of HIPASS J1321–31 (Banks et al. 1999) show a faint ($m_B = 17.1$), dim ($\mu_0^B = 24.2$ mag arcsec^{-2}) galaxy, whose profile is fitted by an exponential law.

A much more detailed view of the dwarf is given by our WFPC2 image (Fig. 19), which shows a very diffuse stellar distribution. There are hardly any lumps or substructures, but one can see two small, bright regions about 2″ across and 7″ apart. It is difficult to tell from the image whether they are HII regions or star clusters, but they are

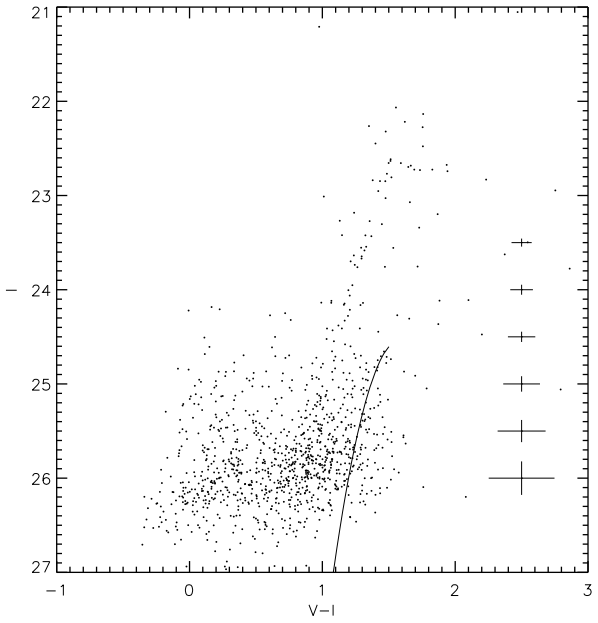

Figure 20. HIPASS J1321-31: $(V - I, I)$ colour magnitude diagram, once again compared with the RGB of the GCC M 15, showing a clear red plume of luminous stars extending up to $I =$ 22.6 mag.

not foreground stars. Given the low column density around the optical counterpart (1 - 2 $\times 10^{20}$ cm^{-2}), the presence of HII regions in this galaxy would be very unusual. If they are regions of SF they were too faint to be detected in the Hα snapshots from the WIYN telescope. It is possible that these are two areas where the SF activity was stronger in the past and which are now "fading".

5.3 The morphology of the CMD

The most striking feature of the CMD of HIPASS J1321–31 is the very unusual red plume which extends at bright magnitudes up to $I \sim 22.6$ with colours $1 < (V - I) < 2$ (Fig. 20) without a corresponding population of bright blue stars. Blue stars have been detected but they reach at most $I = 24$ mag . Among the galaxies of the LG with resolved stellar photometry there is not another object with a similar CMD. Sextans A for example (Dohm-Palmer et al. 1997) does show a bright red plume, but it also has a clear blue plume made of massive stars burning helium in their core, which are evolving into the bluest extent of the so-called 'blue-loop' phase.

The bright red stars of J1321-31 are scattered across the optical extent of the galaxy (Fig. 1 in Pr03), and that seems to indicate that they belong to the dwarf.

Three possible scenarios have been discussed to interpret the nature of these unusual red plume stars in Pr03. At first glance the most obvious option would be that the red plume is the upper extension of the RGB. If so, the tip would be at $I \simeq 22.6$ mag, a much brighter value than the one expected at the distance of the Centaurus A group ($I \sim 24$ mag) and this would place the galaxy in a much closer position to us, at about 2 Mpc. We have ruled out this possibility because:

- the heliocentric velocity of the HI distribution is compatible with the galaxy membership to the Centaurus group;
- if that were the RGB its luminosity function between $I = 22.6$ mag and $I \sim 24.5$ mag would be relatively flat, while the number of stars in the RGB is always found to increase from the tip down to lower magnitudes, even when it appears narrow and sparsely populated as in Leo A (Tolstoy et al. 1998).

We have also excluded that the red plume is made of AGB stars (see Pr03 for details).

We have suggested instead that a more likely scenario for the red plume is that it is populated by core-helium burning stars in the Red Super Giant phase. We can use the comparison with theoretical isochrones and the simulation of CMDs to further constrain the interpretation given in Pr03.

The Padua isochrones can be adjusted to the observed magnitudes of J1321-31 to set age constraints on the different features. We have chosen Z = 0.0004 as the lowest metallicity set after comparing the RGB to that of M 15 (Fig. 20). The lifetime of these stars at such metallicity is around 500 Myr (see Fig. 21,) and their mass is in the range 2 - 3 $M_{\odot}$. The synthetic tracks indicate that the red core helium burning phase would be much brighter while the corresponding blue loop stars would be too faint to be detected in our observations. The presence of the faint blue stars at $-0.1 < V - I < 0.4$ implies that the SF process must have continued after this event, probably at a decreasing rate, and dropped off at an age that can be set around 100 Myr ago (see left panel of Fig. 21).

Adopting a slightly higher metallicity, Z = 0.001 (not shown in the figure), results only in a variation in the age of the red plume, but the overall star formation scenario would be the same. The RSGB stars and those in the blue "hump" would have different ages and correspond to different SF events. The age of the RSGB stars would be around 300 Myr in this case.

With an even higher metallicity (Z = 0.004, right panel of Fig. 21) a 100 Myr old isochrone can fit both the brightest stars of the "blue hump" (with $I < 25.5$) and the red plume. In this scenario, blue and red stars formed at the same time, at a more recent epoch, and the enhancement in the SF dates back to only 100 Myr. However this interpretation seems very unlikely because blue and red plume stars show different spatial distributions: the first are more centrally concentrated (see right panel of Fig. 22) while the latter appear randomly distributed throughout the optical body of the galaxy (Fig. 22, left panel). If both type of stars were coeval it would be difficult to explain their different location within the galaxy. Thus red plume stars have to be older than the blue ones to explain their scatter and we can rule out the higher metallicity (Z = 0.004) scenario.

The constraint on the metallicity of the red plume and the comparison with stellar tracks is the only tool we have at this stage of the analysis to estimate the age of the RGB, that we have defined as the feature located at $1.0 < V - I < 1.7$, extending up to $I \sim 24.5$. If we assume that the metallicity of the plume is Z = 0.0004 - 0.001, we derive the usual scenario of a very low metallicity galaxy with an RGB which is fitted by isochrones as old as 10 Gyr (Fig. 21, left

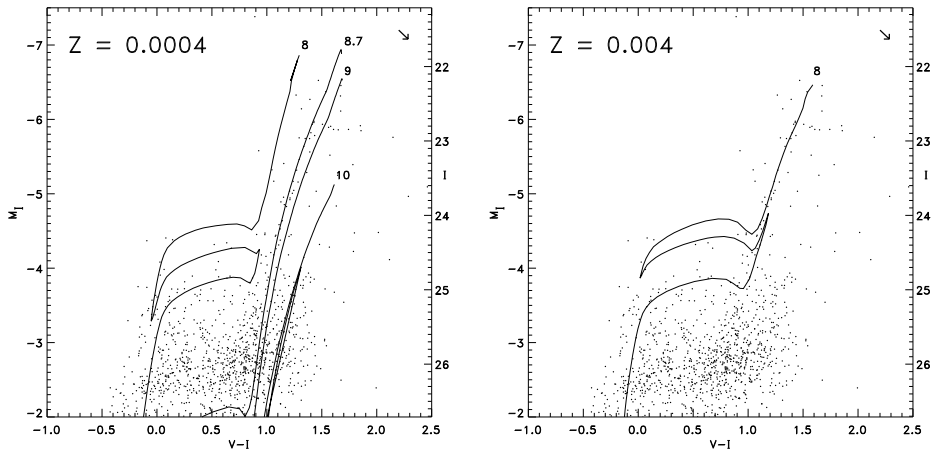

Figure 21. HIPASS J1321-31: dereddened $(V-I,\ I)$ colour magnitude diagrams overlaid on Padua stellar evolutionary tracks at metallicities of Z = 0.0004 and 0.004. For the highest metallicity we show both the isochrone that fits the location of the red plume (to show how the age of the feature may change with the metal abundance) and the oldest isochrone that would set an upper limit to the age of the RGB at that metallicity. The arrows at the top-right corners indicate the reddening vector.

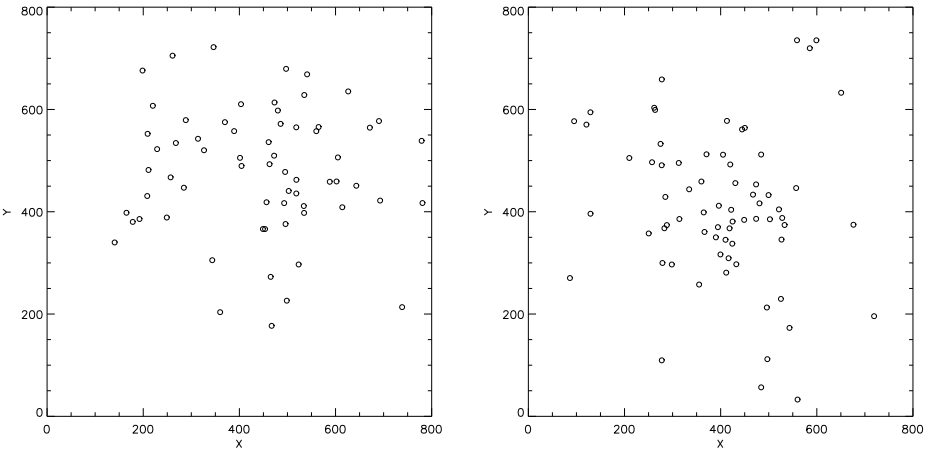

Figure 22. The spatial distribution of the stars in the red plume (*left*) and of the brightest blue ones with $I < 25.5$ (*right*). There is a difference in the distribution of the two populations which suggests that they have been formed at different epochs. Such a difference in location rules out the hypothesis that the red plume has a higher metallicity, Z = 0.004, and that these stars are the redder counterpart of the ones in the blue hump.

panel). The TRGB has been found at $I_0 = 24.43 \pm 0.11$, assuming $E(B-V) = 0.06 \pm 0.01$, with a distance modulus $(m-M)_0 = 28.59 \pm 0.13$, that corresponds to a distance of 5.2 ± 0.3 Mpc (Pr03).

5.3.1 A bursty SFH?

We have modelled the SFH and CMD of J1321-31 with STARFISH, trying different combinations of three sets of isochrones (Z = 0.0004, 0.001, 0.004). The resulting fits obtained for different models are listed in Table 5. Using tracks with Z = 0.0004 and Z = 0.001 yields the best-fit SFH (Fig. 23) and the model CMD (Fig. 24) for comparison with the

Table 5. The list of the different combination of metallicities inspected with STARFISH and the corresponding reduced χ^2 parameter. For HIPASS J1321-31 we find that the best-fit SFH is given by a model with isochrones at Z = 0.0004 and 0.001.

Z	χ^2
0.0004	1.56
0.001	1.41
0.004	1.47
0.0004+0.001	1.30
0.001+0.004	1.40
0.0004+0.001+0.004	1.34

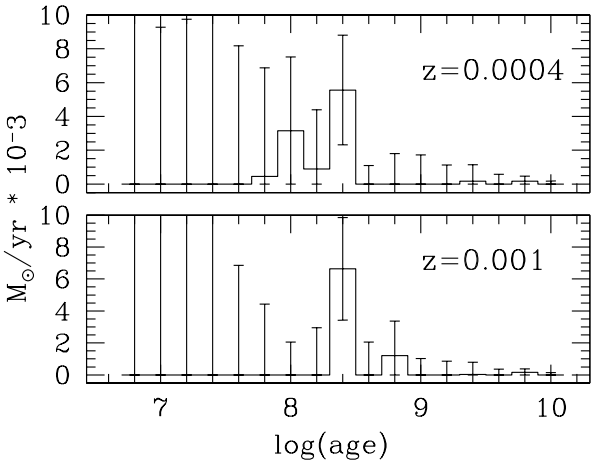

Figure 23. The best-fit SFH of HIPASS J1321–31

observed CMD. We find that a model CMD with metallicity as high as Z = 0.004 cannot reproduce the observed data.

The best-fit SFH suggests that J1321-31 formed its red giant branch at $\log(Age) = 9.8 \pm 0.1$, i.e. the first detectable SF event occurred at $6^{+1.6}_{-1.3}$ Gyr ago. The RGB appears to be relatively "young". This does not exclude the existence of a population of (fainter) stars older than 10 Gyr that we cannot detect, such as HB stars. Also, it appears likely that the algorithm has underestimated the older SFR of the galaxy: the model RGB is less populated than the observed one. There may be some problems in modelling the RGB as the galaxy is more distant than the other dwarfs, thus the stars are closer to the photometric limit and have larger photometric errors.

With regard to more recent SFH, the red plume produced by the code is significantly wider than that observed. In the simulation, the feature begins to appear at $\log(Age) = 8.8$, but the majority of the stars form at $\log(Age) = 8.4$. We would expect the narrow red plume to be the result of a single burst of SF at a single metallicity. However the small number of stars in it made it difficult for the code to model such a sharp burst.

At $\log(Age) = 8.4$ the SFR is about $6 \times 10^{-3} M_\odot$ yr^{-1}, six - ten times higher than the past SF episodes (taking into account the uncertainties on the SFRs). If we use this value to estimate the mass in stars born in the age bin at $\log(Age) = 8.4$, we obtain $M_\star \simeq 7 \times 10^5$ $M_\odot$, which is rather high compared to a luminosity of 7.4×10^6 $L_\odot$. It is possible that the recent SFR is slightly overestimated because the number of predicted blue stars is higher than those observed, nevertheless STARFISH finds that a large fraction of the stellar population was formed in the recent past, and that the galaxy probably went through a "bursty" phase.

On the other hand the enhancement of the SFR that occurred in J1321-31 is not as intense as those found in BCDs. In VII Zw 403 for example, the SFR at its peak was $\sim$ 30 times higher than normal, and the starburst phase lasted for a few hundred million years (Schulte-Ladbeck 1999).

In summary, the simulations of the SFH of J1321-31 have given us the following insights into the SFH of J1321-31:

- Low metallicity isochrones provide a better fit, supporting the hypothesis that the galaxy has an intermediate-age stellar population. As we go back to ages older than 1 Gyr we find that the RGB stars are only about $6^{+1.6}_{-1.3}$ Gyr old.
- The SFR seems to have been significantly higher in the last 500 Myr than it was between 1 and 10 Gyr ago. The red plume originated around 500 Myr ago although the theoretical feature is not as narrow as the one observed.

5.4 Summary and discussion

HIPASS J1321-31 appears to be a very uncommon galaxy both from its gaseous distribution and optical morphology. It has a large amount of HI (with the highest M_{HI}/L_B ratio among the three objects), with a very irregular distribution and low column density ($\lesssim 2.5 \times 10^{20}$ cm^{-2}) which is clearly offset from the optical counterpart.

The stellar distribution is very diffuse and is characterised by bright red stars which are scattered throughout the optical area of the galaxy and form a peculiar red plume when plotted on the CMD. The lack of a corresponding population of bright blue stars indicates that the galaxy has experienced a peculiar star formation history. Three scenarios for the origin of this anomalous red plume were discussed in a previous paper (Pr03) - RGB, AGB, or RSGB stars - and we concluded that it is most probably composed of core helium burning post main sequence stars with ages less than 1 Gyr which are likely to be related to an epoch when the galaxy experienced an increase in the SFR.

To verify this interpretation we have built models of the SFH of the galaxy with different metallicities and found that the best fit was given by assuming a very low abundance for the stellar population (between 1/50 and 1/20 solar) implying, as in the other dwarfs, that the red giant branch is made of intermediate-age stars (< 10 Gyr).

The SFH between 1 and 10 Gyr is characterised by very few events and an overall low SFR (below 2×10^{-3} $M_\odot$ yr^{-1}). We find that the RGB stars are only $6^{+1.6}_{-1.3}$ Gyr old, a few Gyr younger than what we have estimated for the other two dwarfs. Such a low rate is consistent with the scenario of a gas-rich object evolving "slowly", compared to the large amount of gas present (van Zee et al. 1997a).

At more recent ages (< 1 Gyr) the model SFH confirms that the red plume is related to an epoch of increased SFR as we suggested in Pr03. The predicted SFR implies that a large fraction of the stellar population of J1321-31 was produced during this event. The offset of the gas distribution and the interruption of the star formation activity may provide further evidence that the galaxy went through a phase of enhanced SF activity, which heated and pushed away the gas from the optical centre of the galaxy. After this main episode the SFR started to decrease and the SF activity stopped around 100 Myr ago.

As we have done with J1337-3320, an estimate of the metal abundance from the luminosity-metallicity relation may be useful as a comparison to the values used in our simulations. Following Richer & McCall (1995) we obtain $12 + \log(O/H) = 7.4 \pm 0.2$, or $1/45 < Z < 1/15$ of the solar value(again with [Fe/O] = 0). In this case the range of metal abundances obtained from the CMD analysis would be compatible with the luminosity-metallicity relation.

HIPASS J1321-31 appears different from the other two

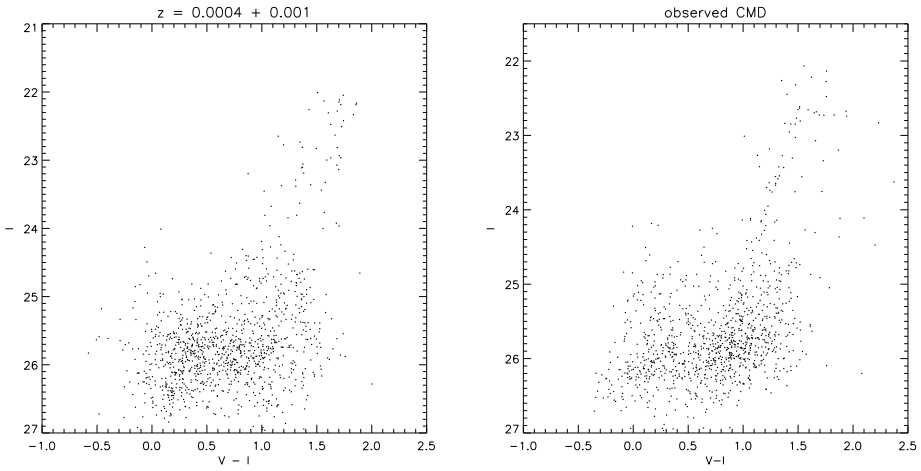

Figure 24. The best-fit model CMD (*left*) of HIPASS J1321–31 obtained using the set of isochrones with Z = 0.0004, 0.0001 is compared to the observed one (*right*).

dwarfs. It is not a young galaxy, formed less than 1 Gyr ago, since we have detected the RGB and have established an age of 6 Gyr for its oldest red giant stars. However it appears to have a predominantly young population with an age less than 500 Myr.

6 DISCUSSION

The high M_{HI}/L_B ratios and low optical luminosity of these dwarfs make them unique objects in the nearby universe. Despite large fractional HI mass they have not used the majority of their gas, and do not show obvious signs of massive SF. We have tried to understand why.

The first issue was to determine if we had found a class of young galaxies, the most natural explanation for their high gas-mass-to-stellar-light ratios. In all the three dwarfs examined, a clear RGB has been detected. There is a difference between the CMDs of these dwarfs and that of I Zw 18, the nearest young galaxy detected so far, with a stellar population that seems to be less than 500 Gyr old, in which a well identified RGB is missing (Izotov & Thuan 2004). The finding of red giant stars in these dwarfs sets a lower limit on their age of at least 1 - 2 Gyr, the minimum time for such stars to appear after a first SF episode. In principle, even much older populations (10 - 12 Gyr) can be found in the RGB, and the presence of a well defined tip, as we have observed in the three dwarfs, is generally considered as a reliable proof for the existence of stars older than 1 - 2 Gyr (Tolstoy et al. 1998).

Secondly, we have looked for AGB stars whose detection would provide unambiguous evidence of an intermediate-age population (1 - 10 Gyr) (Caldwell et al. 1998). Two out of three galaxies (J1337–39 and J1337–3320) do show candidate AGB stars. The lack of AGB stars in J1321–31 is puzzling since we would expect to find such population given that the RGB has been well detected.

Modelling has offered another point of view on the issue. Using the STARFISH code we have found that SF activity between 8 and $\sim$ 12 Gyr ago would explain the appearance of the RGBs in both J1337–39 and J1337–3320. These dwarfs may host older populations of stars which are beyond our detection limits.

The situation is less clear for J1321–31. Its first episode of SF seems to have occurred at $6.3^{+1.6}_{-1.3}$ Gyr ago. The model SFH shows a very weak SFR until about 1 Gyr ago and only in the last 300 Myr we find a significant increase in the SF activity, which then drops again in the last 100 Myr.

Therefore these galaxies are not recently formed objects, and their evolution has proceeded for several Gyrs, most likely with modest episodes of SF activity alternating with periods of very low production of stars or even quiescence.

From their model SFHs we can estimate the average SFR, and we obtain over a 10 Gyr time range the following values: 2×10^{-3} $M_\odot$ yr^{-1} (J1337–39), 0.6 $\times 10^{-3}$ $M_\odot$ yr^{-1} (J1321–31) and 0.2 $\times 10^{-3}$ $M_\odot$ yr^{-1} (J1337–3320).

The HI distributions appear similar to what it is seen in dwarf irregular galaxies (e.g. van Zee et al. 1997b; Young et al. 2003). The neutral gas extend well beyond the optical image, and the peak column density exceeds 10^{21} cm^{-2} only in one case, where there is also a rough correspondence between the HI density peak and regions of current star formation.

The gas depletion time scale $\tau_g \equiv M_{HI}/\mathrm{SFR}$ gives an indication of the time needed to consume the present amount of gas at a given rate. We obtain timescales much longer than the Hubble time ($\sim$ 20, 60, 25 Gyr respectively), therefore these galaxies should be able to retain much neutral hydrogen for several more gigayears.

Another estimate of the formation time scale of these dwarfs is given by their specific star formation rates, i.e. per unit mass of stars, the inverse of the time it would take to form the present stellar mass of a galaxy at a given SFR. The "galaxy-building timescales" for these dwarfs are comparable to the Hubble time (6, 17, 11 Gyr for J1337–39, J1337–3320 and J1321–31 respectively)[5].

We next tried to understand what inhibits the process of SF in these objects, leaving most of the gas un-processed.

[5] Starburst systems for example have typical time scales of 1-2 Gyr, which in certain cases may go down to 0.1-1 Gyr (Heckman et al. 2005).

Is it a consequence of their internal properties – i.e. a too diffuse ISM with low HI column densities, and perhaps the absence of a cold phase of the ISM, with low metallicity and low dust – or is it due to their local environment?

6.1 The role of the gas density and the metallicity of the ISM

Recent work on the gas distribution in dwarf galaxies indicates that their gas densities can be well below the threshold for star formation (Toomre 1964) across the entire stellar disc, suggesting that it is difficult to initiate a global burst of star formation (Hunter & Gallagher 1986; Hunter & Plummer 1996; van Zee et al. 1997b,c; Hunter, Elmegreen, & Baker 1998). The local nature of star formation in dIrr galaxies has been emphasized by Hunter & Gallagher (1986). van Zee (1997b,c; 2001a,b) concludes, after the analysis of several gas-rich dIrr galaxies, that the star formation process in such objects randomly diffuses across the stellar disc, occurring only in those localities where the gas density is sufficiently high to allow molecular cloud formation and subsequent star formation. According to van Zee star formation is a localised phenomenon and it is unlikely that the entire disc will have sufficient gas density to permit a global starburst. Quiescent LSB gas-rich dwarfs show a shallow HI distribution, roughly constant throughout the disc and below 10^{21} cm^{-2}, in contrast to BCDs where the gas is centrally concentrated, and the density peaks are above 10^{21} cm^{-2} (van Zee 2001a).

In our small sample, current SF occurs only in J1337–39, the galaxy where the HI density is highest and above 10^{21} cm^{-2}. This is also the galaxy with the highest average SFR. The other two systems, where the peak column density is about one order of magnitude lower ($N_{HI} \lesssim 2 \times 10^{20}$ cm^{-2}) and the gaseous distribution is almost constant throughout the optical disc, show no signature of current SF.

The low HI surface densities and the low metal content imply that the large amount of gas available for SF may be in a warm phase (T > 100 K), preventing the transition from atomic to molecular hydrogen that cools a gas cloud and leads to its fragmentation. In fact, according to Elmegreen and Parravano (1994) the transition from a warm ($T \sim 10^4$) to a cold phase ($T \sim 100$ K) of the ISM is essential to make the gas gravitationally unstable and trigger SF (see also Elmegreen 2002). Schaye (2004) argues that the phase transition in conditions of local hydrostatic equilibrium, assuming a single phase warm ISM, depends only on the density (and column density) of the gas if the temperature, gas fraction, metallicity and UV radiation field are fixed. SF will occur in those regions where the gas surface density exceeds the local threshold value. Such a critical density correspond to the critical pressure necessary for the existence of a cool diffuse phase. In his model, SF can occur locally only where the pressure is high enough to trigger the phase transition from a warm to a cold medium (Schaye 2004). According to Schaye, at this threshold pressure the surface density is $\Sigma_c \sim 3 - 10 M_\odot$ pc^{-2} (or $N_{H,crit} \sim 3 - 10 \times 10^{20}$ cm^{-2}).

The temperature of the ISM is related to the cooling rate of the gas, which depends on its metal content. The radiative cooling-time of the gas heated by supernovae defines the timescale in which it falls back into the galaxy, where it can eventually be reprocessed in a new SF event. According to Hirashita (2000) the cooling time is given by

$$t_{cool} \sim 7 \times 10^8 \left(\frac{\zeta}{0.1}\right)^{-1} yr \quad (1)$$

where ζ is the metallicity of the galaxy normalized by the solar abundance. According to Hirashita irregular SF activity is common in small size dIrr galaxies and is the consequence of the balance between the heating process of the ISM due to SN, stellar winds and the emission of UV radiation (i.e. stellar feedback) and the cooling rate. Thus the combination of small size (which makes the heating from stellar feedback more effective) and low abundance (determining an inefficient cooling rate) conspire to produce an irregular and "intermittent" SFR in small-size dIrr galaxies (Hirashita 2000).

For our sample of galaxies the metallicity is around 1/20 - 1/50 solar, therefore, from Eq. 1, the cooling times should be between 1.5 and 3.5 Gyr. Therefore their low gas densities and low metal abundances may explain the low SFRs and their "gasping" SFHs.

6.2 The efficiency of SN-driven mass and metal ejection

Establishing that the SF in these dwarfs has occurred for several Gyr raises two more issues. First we should check whether the energy injected into the ISM by SNe and stellar winds, given the derived SFRs, can affect the HI content of these galaxies. Secondly, how can SF activity extended so long in time be consistent with the low metal abundances we have estimated?

Recent models, which include a large dark matter component, have investigated the range of parameters that contribute to the removal of the ISM in a galaxy after an enhanced SF activity, and they show that it is much more difficult to remove the ISM with a single starburst than previously thought (Mac Low & Ferrara 1999, hereafter McF99).

The evolution of a galaxy after an intense SF activity is predicted by McF99 for different gaseous and stellar masses, and for various mechanical luminosities of the starburst L, i.e. the fraction of the total energy released by a supernova into the ISM as mechanical energy, given a certain rate of SNe per year. This parameter is expressed as L_{38} (units of 10^{38} ergs s^{-1}). According to McF99 mass ejection (with the disruption of the gaseous content) is very efficient only for galaxies with $M_{gas+stars} = M_{bar} \lesssim 10^6\ M_\odot$. Galaxies with $M_{bar} \gtrsim 10^7\ M_\odot$ are less affected by starburst events.

To have an idea of the effects on the dwarfs of the most intense SF episodes obtained with STARFISH, we have calculated the L_{38} parameter for each galaxy as in MCF99. The baryonic mass of our dwarf galaxies ranges between $10^7\ M_\odot \lesssim M_{bar} < 10^8\ M_\odot$. Using the dark-to-visible mass ratio ($\phi = M_h/M_{bar}$, where M_h stands for the mass of the dark matter halo) given by Persic et al. (1996) we obtain $35 \gtrsim \phi \gtrsim 20$[6]. We have assumed that the energy released by a SN event is about $E_0 = 10^{51}$ ergs, a tenth of which

[6] Note that this is a factor 2 higher than the dynamical-baryonic-mass ratios found from the velocity widths of the 21-cm emission lines ($20 \gtrsim M_{dyn}/M_{bar} \gtrsim 10$)

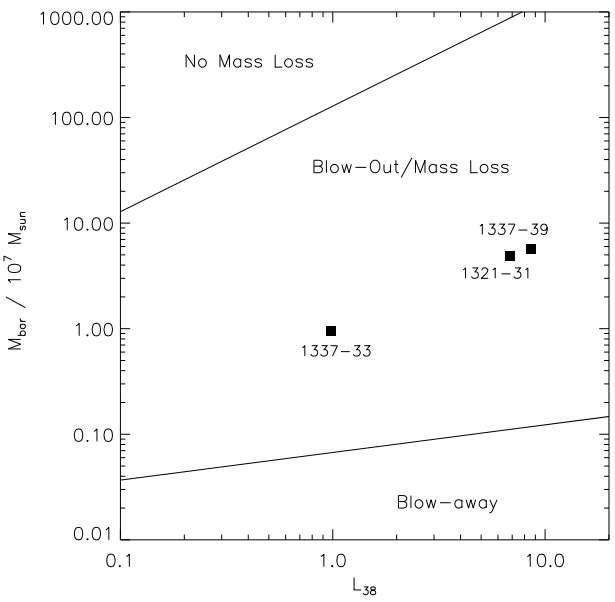

Figure 25. Values of the baryonic mass of a dwarf galaxy and the starburst luminosity showing the regions where blow-away, blow-out or no gas loss may occur (see McF99 for details). The filled squares represent the location on the plane of the HIPASS dwarfs, having considered the most intense SF events in their recent history. As one can see from the picture, all the dwarfs galaxies are in the area of the diagram where only blow-out may occur, i.e. only the hot enriched gas is ejected. The episodes of SF are not able to eject the whole ISM and the galaxies according to the McF99 model are able to retain the bulk of their gas content.

is deposited into the ISM while the rest is radiated away (Thornton et al. 1998) We have estimated the amount of stellar mass produced in the SF episodes with the highest SFR for each dwarf in their recent past where the time resolution of the SFH is higher (for example for J1321–31 we have considered the event at log(Age) = 8.4, for J1337–39 the most recent event at 10 Myr, and for J1337–3320 the one at log(Age) = 7.8). We have then calculated the number of SNe produced in each SF event (N_{SN}), using a Salpeter mass function, and derived L_{38} as $N_{SN}E_0/10\Delta t$ where Δt is given by the width of the corresponding age bin. We have then plotted the results in the M_{bar} - L_{38} plane as defined in McF 99 (Fig. 25).

As one can see from the figure, all the three dwarfs are included in the area of the plane labelled as *Blow-Out/Mass Loss* where they undergo blow-out of the gas, but where the ISM will not be completely ejected.

According to the simulations of McF99, the effect of the stellar winds and SNe on the metal abundances is much more dramatic. About 60% of the metal-enriched material is expelled from a galaxy with $M_{bar} = 10^9\ M_\odot$, a fraction that increases up to 100% for $M_{bar} = 10^8\ M_\odot$, which is the order of magnitude of the total baryonic mass of our dwarfs. Metals easily escape from low mass dwarf galaxies because the chemically enriched material produced by the stars is entrained within the hot bubble of gas where it reaches the edge of the galaxy and the sound speed is higher than the escape velocity (Legrand 2000).

On the other hand, if a low mass dwarf galaxy experiences low luminosity SF events, with a lower rate of SNe, the outflow of the metal-enriched gas into the intergalactic medium may be reduced (McF99; Ferrara & Tolstoy 2000) leading to a gradual increase in the metal abundance of its ISM. This is what may have happened in J1337–3320, which is the galaxy with a higher metallicity among the three dwarfs, and a lower average SFR, and it seems to show two stellar populations with different chemical abundance. Its ISM may have been chemically enriched by the older generation of RGB stars and the metals may have been reprocessed into the later SF events.

6.3 The effects of the environment

M 83 is the closest massive spiral to the HIPASS dwarfs, and we have calculated their location and dynamical status in relation to this bright galaxy to check if there is a possible connection between the environment of the dwarfs and their observed properties. The distance from M83 is assumed to be

$$R^2 = D^2 + D^2_{M83} - 2D \cdot D_{M83} cos\theta \qquad (2)$$

where θ is the angular separation from M 83, D the distance of each dwarf derived from its TRGB and D_{M83} = 4.5 Mpc.

Excluding J1337–3320 ($R \sim 300$ kpc), the location of the other two dwarfs in the group seems similar to those of dIrrs in the LG such as WLM, SagDIG or Gr 8, at about 850 kpc (J1337–39) and 800 kpc (J1321–31) from the more massive galaxies of the group.

Being in the outskirts of the group the triggering of frequent star formation events through collisions or tides in the discs of J1337–39 and J1321–31 may not have occurred. This could be advanced as an additional explanation for their 'retarded' evolution. Because of its relative closeness to M 83, the case of J1337–3320, which indeed has the lowest M_{HI}/L_B of the three, is slightly different.

Gas-rich dIrr galaxies are found in the LG, but the main difference from the HIPASS dwarfs is that they are not as gas-rich. Their M_{HI}/L_B ratios in fact are in general around or below 1. We may wonder if one of the reasons why we do not find this type of dwarf galaxy in the LG is because of an intrinsic difference between the two environments.

In Fig. 26 we compare the gas fractions of the smaller members of the LG, Sculptor and Centaurus A as a whole group[7], without including their primary galaxies. The HI sources in Centaurus A have been taken from Côté (1997), Banks (1999), and Karachentsev et al. (2002), and the updated fluxes have been extracted by the HIPASS brightest galaxy catalogue (Koribalski et al. 2004). The reddening corrected optical magnitudes have been taken from the Nasa Extragalactic Database (NED). The M_{HI}/L_B ratios for the dwarfs of the LG come from Mateo (1998). For Sculptor the objects have been taken from SCM03, Karachentsev et al. (2003) and Bouchard et al.

[7] For those members for which distances are not known, it is not possible to distinguish whether they belong to the Cen A or M 83 subgroup. Therefore for this comparison we consider Centaurus A as a single group

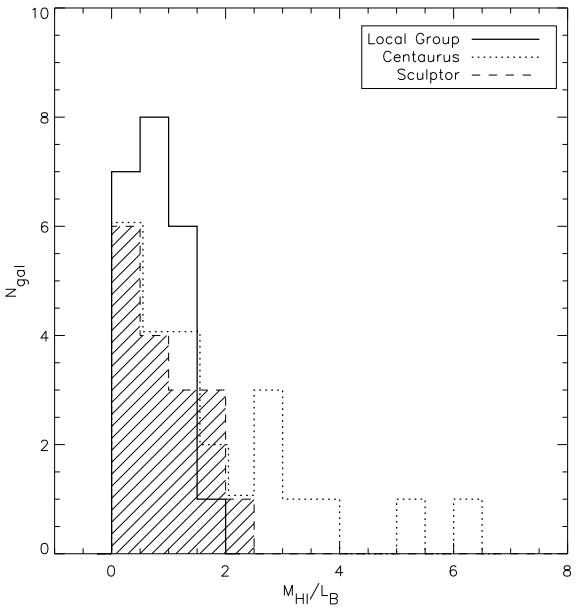

Figure 26. The comparison between the M_{HI}/L_B ratios of 24 galaxies in the Centaurus A group (*dotted line*), 22 galaxies in the LG (*solid line*), and 17 galaxies in Sculptor (*dashed line*). As one can see the majority of the galaxies in the LG have ratios less than 1.5, while the sample of the Centaurus A and Sculptor galaxies extend to higher M_{HI}/L_B ratios.

(2005). Some of the objects with the higher M_{HI}/L_B ratios in SCM03, such as Sc 18 and Sc 24, have revealed to be false detections (Karachentsev et al. 2003) and have not been included in the list. For other objects with high M_{HI}/L_B ratios such values have been recalculated using the more recent data from the HIPASS brightest galaxy catalogue and HOPCAT, the optical counterparts for HI radio-selected galaxies (Doyle et al. 2005), giving smaller values than those in SCM03.

As one can see in the Figure, 95% of the satellites of the LG have M_{HI}/L_B ratios below 1.5 in solar units, against $\sim$ 60% of the objects in Cen A. The remaining 40% have much higher M_{HI}/L_B ratios up to ~ 6 (see also Knezek 1999). The higher average number of gas-rich satellites does not seem to be the consequence of the different crossing time. Comparing the subgroups formed by the Milky Way and M83, Karachentsev et al. (2002) find that the velocity dispersion of the the M83 satellites correspond to a crossing time of 2.3 Gyr, while in the Milky Way it is 2.1 Gyr (Karachentsev 2005). Graham (1976) and van Gorkom et al. (1990) tried to explain this issue suggesting that the Centaurus A complex has recently accreted a population of gas-rich dwarfs, but the velocity dispersion of its members, typical of groups of galaxies of this size, does not seem to justify this interpretation (Knezek 1999). Moreover, the group is well known to be gas-rich at all luminosities (Knezek 1999; Banks et al. 1999), since even its early-type systems such as NGC 5102 and NGC 5128 are very gas-rich for their types. Therefore there does not seem to be an obvious explanation to justify the difference in the gas content between the Centaurus A complex and the LG. Sculptor also contains gas-rich objects (about the 25% of the smaller galaxies detected at 21-cm have $M_{HI}/L_B > 1.5$). The group is known to be a loose aggregation of galaxies – extending for about 6 Mpc along the line of sight – and it does not seem to be a a virialized system given its long crossing time – 6.9 Gyr for the bigger subgroup centered around NGC 253 (Karachentsev et al. 2003). Therefore, interaction between galaxies are expected to be low and external gas stripping largely ineffective in Sculptor, yet the gass-mass-to-light ratios are not as high as those found in CentaurusA/M83.

6.4 Comparison with other dwarf and irregular galaxies

6.4.1 Similar objects within the LG

The stellar populations of most dwarfs in the LG have been studied in detail, therefore the comparison with these systems may give further hints on the understanding of our gas-rich dwarfs.

Sag DIG is probably the galaxy that most resembles J1337–39 and it is gas-rich with $M_{HI}/L_B = 1.6$. It is considered the most remote object belonging to the LG, since it is located at a distance of 1.29 $\pm$ 0.09 Mpc from the LG barycenter (van den Bergh 2000b). From its RGB Sag DIG appears the most metal poor dIrr of the LG ([Fe/H]= –2.1 $\pm$ 0.2) (Momany et al. 2002). The youngest stars are located near the major peaks of emission in the HI distribution (which appears as a complete asymmetric ring with a central depression), whereas the red giants and intermediate-age AGB stars define an extended halo or disc with scale length comparable to the size of the hydrogen cloud. The CMD of this fairly gas-rich dwarf obtained by Momany and collaborators (2002) has many features in common with that of J1337–39: the well populated blue plume, the blue RGB typical of a low metallicity population, and the evidence for AGB stars above the TRGB. Deeper observations carried out with the Advanced Camera for Surveys (ACS) on the HST (Momany et al. 2005) show also the presence of a red HB, proving that SF started around 10 Gyr ago in this galaxy.

Therefore dIrr galaxies in the LG do contain an ancient ($\gtrsim$ 10 Gyr) stellar population. HB stars have been detected also in WLM ($M_B = -13.9$; $M_{HI}/L_B = 1.2$; Mateo 1998) and it is the only dwarf that contains a globular cluster (Hodge et al. 1999). The time of initial SF has been set at about 12 Gyr ago (Dolphin 2000b), again showing that isolated and fairly gas-rich dIrr galaxies of the LG have experienced SF even at ancient epochs.

The general properties of the remaining two galaxies, J1337–3320 and J1321–31, such as the low luminosity, the spherical symmetry of the optical appearance, the absence of current SF activity despite the large gas reservoir, make these dwarfs more similar to the so called "transition objects" of the LG such as LGS 3, Antlia, Pegasus (Miller et al. 2001; Gallagher et al. 1998; Lee et al. 1999). All these galaxies have low luminosities ($M_B = -9.9$; -10.2; -12.3) and M_{HI}/L_B less than 1 in solar units. They are among the lowest mass objects ($M_\star \gtrsim 10^6\ M_\odot$) which have been able to retain gas and to experience SF until a few hundred million years ago and they show how the process of gas consumption and quiescence takes place in dwarf galax-

ies. Moreover they are within 300 - 400 kpc from either the Milky Way or M 31.

According to Gallagher et al. (1998), SF in Pegasus ($M_{HI}/L_B = 0.2$) is temporarily "down", but it is not excluded that it could re-establish a normal level of SFR in future. The prominent RGB and the extended AGB indicate that the SF at intermediate-ages was more intense than during its more recent history. This galaxy may be taken as an example of "gasping" SFH, since it appears to have experienced occasional intense episodes of SF in its past, lasting for 0.5 - 1 Gyr, followed by more quiescent phases, lasting one to few Gyr (Cole et al. 1999).

LGS 3, in the M 31 subgroup, with its smooth gaseous and stellar distribution is probably the galaxy that most resembles J1337–3320. Its SFH appears not to have been characterised by strong bursty events. After an early event around 13 - 15 Gyr it has been followed by a uniform and low SFR (around 10^{-4} $M_\odot$ yr^{-1}) (Miller et al. 2001). The smooth chemical enrichment of the stellar population suggests that there have not been sufficiently violent bursts of SF to expel a large fraction of the metals, which instead have been reprocessed into stars.

Finding a galaxy in the LG with properties similar to J1321–31 is difficult, but its relative isolation and recent drop in the SF activity, make DDO 210 a good candidate. DDO 210 shows a low luminosity ($M_B = -10.95$) and is fairly gas-rich ($M_{HI}/L_B = 0.87$) (Young et al. 2003). Its current SFR is negligible, but it shows an enhancement in the last few hundred million years compared to the average value for its entire lifetime (Lee et al. 1999). There is evidence of SF until 30 Myr ago (Lee et al. 1999), however the recent drop of SF is puzzling because it contains large amounts of cold neutral gas (at low velocity dispersion of 3 - 5 km s^{-1}) with peak density as high as 10^{21} cm^{-2} (roughly one order of magnitude higher than J1321–31) (Young et al. 2003).

6.4.2 Comparison with gas-rich galaxies outside the Local Group

Beyond our Local Group, Sculptor is the closest system of galaxies hosting few objects with high M_{HI}/L_B ratios (Cotê et al. 1997), whose SF properties have been recently studied by SCM03. Their SFR, normalised to the galaxy luminosity or gas mass, indicates that these dwarfs are experiencing modest SF activity compared to the LG objects, and they show long gas depletion time scales (in some cases $\tau_{gas} >$ 100 Gyr) (SCM03). However among the new gas-rich galaxies discovered by Cotê et al. (1997), those with the most extreme properties (very low SFRs and $\tau_{gas} \sim 1000$) such as Sc 18 and Sc 24 turned out to be false detections (Karachentsev et al. 2003). The low density of the Sculptor environment, where interactions between galaxies are expected to be minimal and external gas stripping largely ineffective, is probably the most plausible reason to explain the properties of these galaxies. As mentioned in sec 6.3, the group contains also three 'transition' (dSph/dIrr) galaxies, which have fainter luminosities compared to the other gas-rich objects in the group and they show no sign of current SF activity.

The Sculptor gas-rich galaxies tend towards larger gas fractions and lower SFR as the three dwarfs we have analysed, while the dIrrs in the LG are not unusually gas-rich and show higher relative SFRs (SCM03). Nevertheless the Sculptor dIrrs cover a higher range of luminosities when compared to the HIPASS dwarfs (Fig. 27). The properties of our sample are on average more similar to the Sculptor transition type objects, even though they seem to have different spatial distribution within the groups and larger M_{HI}/L_B ratios.

A sample of high HI mass-to-light ratio galaxies has been recently studied by Warren et al. (2006), obtaining more accurate measurements of the M_{HI}/L_B parameter. Warren and collaborators show that the estimates of this ratio based on magnitudes in available catalogues often turn out to be too high. After the new optical observations only three out of nine galaxies have $M_{HI}/L_B > 3$, including one extremely gas-rich object, ESO 215-G?009. The sample does not include only dIrrs but also different morphological types of galaxies much brighter and with a high gas content than the dwarfs we have studied. However it is interesting to underline some properties in common with our sample such as their isolation in space, the extended HI discs and the low density of the gas, factors that as we have discussed in the previous sections prevent a vigorous SF activity.

In Fig. 27 we compare the B absolute magnitude and the HI mass of the HIPASS dwarfs to the dIrrs of the LG (§6.4.2) and the gas-rich objects we discussed in this section, i.e. the Sculptor galaxies and the sample of Warren et al. (2006). We also show the isolated LSB galaxies from van Zee (1997b) characterised by high M_{HI}/L_B ratios and long gas depletion time scales. However, as one can see from the figure, this sample covers a range of properties (luminosity, gas masses and also optical morphology) which is remarkably different from the dwarfs in Centaurus A.

7 CONCLUSIONS

Nearby dwarf galaxies are one of the best environments in which to study in detail how stellar evolution proceeds. Accurate analysis of their resolved stellar photometry (when feasible) and of their gas content (if present) is essential for a better understanding of the internal processes that influence the SF evolution of a galaxy, such as the metal abundance and the density of the ISM, or external effects, such tidal interaction or merging.

Dwarf galaxies in the LG all show varied and very complex SFHs. Dwarfs are all unique objects: it is difficult to find a common pattern in their evolution. It appears that SF has occurred either continuously over long period of time or, in a few objects such as Carina or Sculptor, in distinct episodes (Grebel 1997). All LG galaxies for which sufficiently deep photometry is available do seem to contain at least an intermediate-age population of stars, and for the majority of them old populations of stars have been uncovered. Therefore SF started in the LG at an epoch comparable to the Hubble time.

But what do we know about other groups? Do dwarf galaxies outside the LG behave in the same way? Have they formed at the same time as in the LG? In order to get a complete overview of the evolution of dwarfs we need to extend the same analysis to nearby environments.

This was one of the aims of this study even though the observational limits are challenging. Studies of dwarf galax-

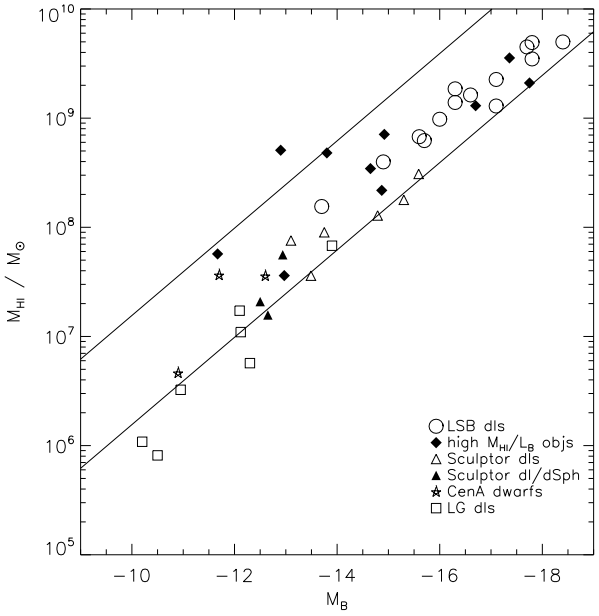

Figure 27. The B absolute magnitude and the HI mass of the HIPASS dwarfs (*stars*) are compared to the LG dIrrs (*open squares*), the Sculptor dIrrs (*open triangles*) and transition-type galaxies (*filled triangles*), the sample of high M_{HI}/L_B objects from Warren et al. (2006) including also DDO 154 (M_{HI}/L_B = 9.4) and UGC292 ($M_{HI}/L_B = 7$) (*filled diamonds*), and the isolated LSB galaxies from van Zee (1997b) (*big circles*). The lines correspond to $M_{HI}/L_B = 1$, 10.

ies outside the LG have been already carried out, but they have been mostly restricted to objects with different properties from our sample, such as luminous BCDs going through an intense period of SF activity (SchulteLadbeck et al. 1999; 2001; Annibali et al. 2003; Cannon et al. 2003; Izotov & Thuan 2004). Instead the HIPASS dwarfs with their large gas fractions, their low masses, SBs and faint luminosities, give an insight into a different evolutionary environment, where galaxies can evolve in a smooth and more quiescent way.

While we do find signs of an intermediate-age population, showing that SF occurred several Gyr ago, much deeper data is needed to verify that the SF activity started in these galaxies at the same time as in the LG dwarfs, and yet the detection of such stars would be very challenging.

The idea that very small galaxies should experience a single primary and possibly cataclysmic episode of SF during their lifetimes does not appear to fit the HIPASS dwarfs we have studied, in analogy with what is found in the LG. We have pointed out that according to recent simulations (MCF99; Ferrara & Tolstoy 2000), their ISMs seem to be stable to SF events even if they happen to be fairly strong, as we have found in J1321–31. The HIPASS dwarfs show that low mass galaxies can retain their ISM even if they have experienced SF activity for several Gyr. We have also shown that if their evolution were to proceed at the same average rate that they have experienced so far, it will take at least another Hubble time to consume all their gas.

Therefore it seems unlikely that these objects will become dSphs. Their evolutionary rate is too slow and their positions within the group too isolated to reach the SFR necessary to burn all the hydrogen. With a hydrogen mass of about 10^7 $M_\odot$ they would need to reach a SFR of 10^{-2} $M_\odot$ yr^{-1} and to maintain it for 1 Gyr in order to consume their gaseous fuel. This seems highly unlikely given their SFHs. Moreover the low gaseous density, and the inefficiency of the cooling mechanism due to the low metallicity would prevent the possibility of a long SF period at a high rate. Shorter episodes of SF activity would require higher rates of 10^{-1} $M_\odot$ yr^{-1} for 100 Myr.

This is in agreement with what is found in the LG, where gas removal in dwarf spheroidals appears to be the combination of internal processes (a relatively rapid initial and intermediate-age SF activity that reduced the gas supplies) and external factors (the stripping of the depleted gas disc by a close encounter with a giant galaxy) (Grebel, Gallagher & Harbeck, 2003).

Is it possible for these galaxies to go through a starburst phase turning into BCDs? One of the key question of dwarf galaxy evolution is whether there is a link between starbursting systems and quiescent gas-rich galaxies, whether they are the same objects viewed at different stages of their evolution. Gas-rich galaxies in principle have large reservoir of gas to ignite intense SF activity. However according to van Zee the majority of gas-rich dIrr do not go through a starburst phase. This is mainly the consequence of different intrinsic properties between gas-rich dIrrs and BCDs (van Zee 2001b). BCDs have steeper rotation curves and lower angular momenta, which lead to centrally concentrated, high density gas distribution favouring the triggering of a starburst. From the simulation of the SFH we have found only in HIPASS J1321–31 a significant increase in its past SFR (between six an ten times the SFR from 1 to 10 Gyr, taking into account the uncertainties on the SFR values). It is difficult to say whether J1321–31 has experienced a BCD phase or not, although the enhancement in the SF is probably not strong enough. It seems unlikely that the HIPASS dwarfs went through a starburst phase in their past, suggesting that factors other than richness in gas have to play role in the triggering of a BCD phase in dwarf galaxies.

We are still left with the intriguing issue of what prevents the conversion of the gas content of a galaxy into stars. We have suggested some possible mechanisms that may be responsible for the observed *"retarded"* evolution of the dwarfs found in the Centaurus A group. Understanding the characteristics of the ISM and the conditions of the local environment may be crucial in order to infer why SF is inefficient in these dwarfs. Our analysis of the resolved stellar populations and the gaseous distributions goes in this direction and allows us to examine the correlation between neutral gas and star forming regions, and to estimate the timescale of the main evolutionary episodes of the history of these galaxies, as well as their location within the group. However a complete understanding of what prevents stars from forming in these environments is still missing.

The next stage of this analysis is to extend the study of the stellar populations of gas-rich galaxies to a much larger and more varied sample. A first obvious target would be the Sculptor group where similarly high gas-mass-to-stellar-light ratios have been measured in few objects (SCM03), with the advantage of being closer than Centaurus A. The analysis of another group would allow to investigate how different

environmental conditions can be related to the evolution of gas-rich galaxies.

ACKNOWLEDGEMENTS

We would like to thank Erwin de Blok for his help with the ATCA observations. BJP, PMK, and JSG are pleased to acknowledge support for this work through NASA funds supplied by the Space Telescope Science Institute. This research has made use of the NASA/IPAC Extragalactic Database (NED), which is operated by the Jet Propulsion Laboratory, California Institute of Technology, under contract with the National Aeronautics and Space Administration.

REFERENCES

Albert L., Demers S., Kunke, W.E., 2000, AJ, 119, 2780
Annibali F., Greggio L., Tosi M., Aloisi A., Leitherer C., 2003, AJ, 126, 2752
Banks G.D., et al., 1999, ApJ, 524, 612
Battinelli P., & Demers S., 2000, AJ, 120, 1801
Bertelli G., Bressan A., Chiosi C., Fagotto F., Nasi E., 1994, A&AS, 106, 275 (Be94)
Bouchard A., Jerjen H., Da Costa G.S., Ott J., 2005, AJ, 130, 2058
Boyce P.B., et al., 2001, ApJ, 560, L127
Caldwell N., Armandroff T.E., Da Costa G.S., & Seitzer P., 1998, AJ, 115, 535
Cannon J.M., Dohm-Palmer R.C., Skillman E.D., Bomans D.J., Côt S., Miller B.W., 2003, AJ, 126, 2806
Cardelli J.A., Clayton, G.C., Mathis J.S., 1989, ApJ, 345, 245
Carraro G., Chiosi C., Girardi L., & Lia C., 2001, MNRAS, 327, 69
Cole A.A., et al., 1999, AJ, 118, 1657
Cook K.H., 1987, PhD Thesis, Arizona Univeristy, Tucson
Cooper B.F.C., Price R.M., Cole D.J., 1965, AuJPh, 18, 589
Côté S., Freeman K.C., Carignan C., & Quinn P., 1997, AJ, 114, 1313
Da Costa G.S., & Armandroff T.E., 1990, AJ, 100, 162
de Vaucouleurs G., 1975, in Galaxies and the Universe, eds. A. Sandage, M. Sandage, & J. Kristian Chicago Univeristy Press, 557
de Vaucouleurs G., 1979, AJ, 84, 1270
Deharveng J.M., Jedrzejewski R., Crane P., Disney M.J., Rocca-Volmerange B., 1997, A&A, 326, 528
Demers S., & Battinelli P., 2002, AJ, 123, 238
Dohm-Palmer R.C., et al., 1997, AJ, 114, 2514
Dolphin A., 2000a, PASP, 112, 1397
Dolphin A., 2000b, ApJ, 531, 804
Doyle M.T., et al., 2005, MNRAS, 361, 34
Elmegreen B.G., Parravano A., 1994, ApJ, 435, L121
Elmegreen B.G., 2002, ApJ, 577, 206
Ferrara A., Tolstoy E., 2000, MNRAS, 313, 291
Gallagher J.S., Tolstoy E., DohmPalmer R.C., 1998, AJ, 115, 1869
Girardi L., Bertelli G., Bressan A., Chiosi G., Groenewegen M.A., Marigo P., Salasnich B., Weiss A., 2002, A&A, 391, 195 (Gi02)
Graham J.A., 1976, AJ, 81, 681
Grebel E.K., 1997, RvMA, 10, 29
Grebel E.K., Gallagher J.S., Harbeck D., 2003, AJ, 125, 1926
Grevesse N., & Sauval A.J., 1998, Space Science Reviews, 85, 161
Hamuy M., Walker A.R., Suntzeff N.B., Schommer R.A., Aviles R., 1992, PASP, 677, 533
Hamuy M., Philips M.M., Maza J., Suntzeff N.B., Schommer R.A., Aviles R., 1994, PASP, 700, 566
Harris G.L.H., Poole G.B., Harris W.E., 1998, AJ, 116, 2866
Harris J., & Zaritsky D., 2001, ApJS, 136, 25
Heckman T.M., et al., 2005, ApJ, 619, L35
Hirashita H., 2000, PASJ, 52, 107
Hodge P.W., Miller B.W., 1995, ApJ, 451, 176
Hodge P.W., Dolphin A.E., Smith T.R., Mateo M., 1999, ApJ, 521, 577
Holtzman J.A., Burrows C.J., Casertano S., Hester J.J., Trauger J.T., Watson A.M., Worthey G., 1995, PASP, 107, 1065
Hunter D.A., Gallagher J.S., 1986, PASP, 98, 5
Hunter & D.A., Plummer J.D., 1996, ApJ, 462, 732
Hunter D.A., Elmegreen B.G., Baker, A.L., 1998, ApJ, 493, 595
Hunter D.A., & Elmegreen B.G., 2004, AJ, 128, 5
Iben I Jr., Renzini A., 1983, ARA&A, 21, 217
Izotov Y. I., & Thuan T. X. 1999, ApJ, 511, 639
Izotov Y.I., & Thuan T.X., 2004, ApJ, 616, 768
Jerjen H., Binggeli B., & Freeman K.C., 2000a, AJ, 119, 593
Jerjen H., Freeman K.C., & Binggeli B., 2000b, AJ, 119, 166
Junkes N., Haynes R.F., Harnett J.I., Jauncey D.L., 1993, A&A, 269, 29
Karachentsev I.D., 1996, A&A, 305, 33
Karachentsev I.D., et al., 2002, A&A, 385, 21
Karachentsev I.D., et al., 2003, A&A, 404, 93
Karachentsev I.D., 2005, AJ, 129, 178
Kilborn V.A. et al., 2002, AJ, 124, 690
Knezek P.M., 1999, PASA, 16, 60
Koribalski B., et al., 2004, AJ, 128, 16
Landolt A.U., 1992, AJ, 104, 340
Lang R.H., et al. 2003, MNRAS, 342, 738
Lee M.G., Freedman W.L., & Madore B.F., 1993, ApJ, 417, 553
Lee M.G., Aparicio A., Tikonov N., Byun Y., Eunhyeuk K., 1999, AJ, 118, 853
Legrand F., 2000, A&A, 354, 504
Lo K.Y., Sargent W.L.W. & Young K., 1993, AJ, 106, 507
Mac Low M.M., & Ferrara A., 1999, ApJ, 513, 142 (McF99)
Madore B.F., & Freedman W.M., 1995, AJ, 109, 1645
Massey P., Strobel K., Barnes J.V., Anderson E., 1988, ApJ 328, 315
Mateo M.L., 1998, ARA&A, 36, 435
McGaugh S.S., 1991, ApJ, 380, 140
Meyer M.J., et al., 2004, MNRAS, 350, 1195
Miller B.W., Dolphin A.E., & Hodge P., 2001, ApJ, 562, 713
Minchin R.F., et al., 2003, MNRAS, 346, 787
Minchin R.F., et al., 2004, MNRAS, 355, 1303
Momany Y., Held E.V., Saviane I., & Rizzi I., 2002, A&A, 384, 393
Momany Y., et al., 2005, A&A, 439, 111
Osterbrock D.E., 1989, *Astrophysics of Gaseous Nebulae and Active Galactic Nuclei*, Mill Valley Univ. Science Books
Pagel B.E.J., Edmunds M.G., Blackwell D.E., Chun M.S., Smith G., 1979, MNRAS, 189, 95
Persic M., Salucci, P. Stel, F., 1996, MNRAS, 281, 27
Pilyugin L.S., 2000, A&A, 362, 325
Pilyugin L.S., 2001a, A&A, 373, 56
Pilyugin L.S., 2001b, A&A, 374, 412
Pritchet C., 1979, ApJ, 231, 354
Pritzl B.J., et al. 2003, ApJ, 596, L47 (Pr03)
Richer M.G., & McCall M.L., 1995, ApJ, 445, 642
Roberts M.S., & Heynes M.P., 1994, ARA&A, 32, 115
Saha A., Sandage A., Labhardt L., Schwengeler H., Tamman G.A., Panagia N., Macchetto F.D., 1995, ApJ, 438, 8
Schaye J., 2004, ApJ, 609, 667
Schlegel D.J., Finkbeiner M.D., Davis M., 1998, AJ, 500, 525
Schulte-Ladbeck R.E., Hopp U., Greggio L., Crone M.M., 1999, AJ, 118, 2705
Schulte-Ladbeck R.R., Hopp U., Greggio L., Crone M.M., Drozdovsky I.O., 2001, AJ, 121, 3007
Simpson C.E., & Gottesman S.T., 2000, AJ, 120, 2975
Skillman E.D., Kennicutt R.C., Hodge P.W., 1989, ApJ, 347, 875

Skillman E.D., 1989, ApJ, 347, 883
Skillman E.D., Côté S., Miller B.W., 2003, AJ, 125, 610 (SCM03)
Soria R., et al., 1996, ApJ, 465, 79
Stetson P.B., 1987, PASP, 99, 191
Stetson P.B., 1994, PASP, 106, 250
Telesco C.M., & Harper D.A., 1980, ApJ, 235, 392
Thim F., Tamman G.A., Saha A., Dolphin A., Sandage A., Tolstoy E., Labhardt L., 2003, ApJ, 590, 256
Thornton K., Gaudlitz M., Janka H.-Th., Steinmetz M., 1998, ApJ, 500, 95
Tolstoy E., et al., 1998, AJ, 116, 1244
Toomre A, 1964, ApJ, 139, 1217
Tully R.B., 1987, ApJ, 321, 280
van den Bergh S. 1959, , Pub. David Dunlap Obs., 2, 159
van den Bergh S., 1980, PASP, 92, 122
van den Bergh S., 1999, AJ, 117, 2211
van den Bergh S., 2000a, AJ, 119, 609
van den Bergh S., 2000b, PASP, 112, 529
van Driel W., KraanKorteweg R.C., Binggeli B., & Huchtmeier W.K., 1998, A&A, 127, 397
van Gorkom J.H., van der Hulst J.M., Haschick A.D., Tubbs A.D., 1990, AJ, 99, 1781
van Zee L., Haynes M.P., Salzer J.J., Broeils A.H., 1997a, AJ, 113, 1618
van Zee L., Haynes M.P., Salzer J.J., 1997b, AJ, 114, 2479
van Zee L., Haynes M.P., Salzer J.J., 1997c, AJ, 114, 2497
van Zee L., 2001a, AJ, 121, 2003
van Zee L., 2001b, AJ, 122, 121
Warren B.E., Jerjen H., Koribalski B.S., 2004, AJ, 128, 1152
Warren B.E., Jerjen H., Koribalski B.S., 2006, AJ, 131, 2056
Wilcots E.M.,& Miller B.W., 1998, AJ, 116, 2363
Young L.M., & Lo, K.Y., 1996, ApJ, 462, 203
Young L.M., & Lo, K.Y., 1997, ApJ, 490, 710
Young L.M., van Zee L., Lo K.Y., Dohm-Palmer R.C., Beierle M.E., 2003, ApJ, 592, 111
Zwaan M.A., et al. 2004, MNRAS, 350, 1210